

Conf. 720701--3

To be presented at the Conference on Nuclear Structure Study with Neutrons, Budapest, Hungary, July - August 5, 1972)

THE OPTICAL MODEL*

G. R. Satchler and F. G. Perey
Oak Ridge National Laboratory
Oak Ridge, Tennessee, U.S.A.

NOTICE

This report was prepared as an account of work sponsored by the United States Government. Neither the United States nor the United States Atomic Energy Commission, nor any of their employees, nor any of their contractors, subcontractors, or their employees, makes any warranty, express or implied, or assumes any legal liability or responsibility for the accuracy, completeness or usefulness of any information, apparatus, product or process disclosed, or represents that its use would not infringe privately owned rights.

1. Introduction

Aside from its intrinsic interest, the optical model of the scattering of neutrons from nuclei has a number of practical uses. It allows one to correlate large amounts of data on elastic scattering, absorption, and total cross sections and hence to predict by extrapolation the cross sections for targets or energies as yet unmeasured. Through the introduction of the Hauser-Feshbach and/or direct interaction formalisms, this predictive power may be extended to inelastic scattering and some other reactions.

There are several theoretical ways of viewing the optical potential U . A simple physical picture is given by the expression

$$U(\vec{r}) = \left[\int \rho(\vec{r}_i) v(\vec{r}, \vec{r}_i) d\vec{r}_i + \text{exchange terms} \right] \quad (1)$$

+ terms of order v^2 and higher,

where $v(\vec{r}, \vec{r}_i)$ is an effective interaction between the projectile nucleon at \vec{r} and a target nucleon at \vec{r}_i , while $\rho(\vec{r}_i)$ is the density distribution of the target nucleons. This v is essentially the Brueckner-Bethe

*Research sponsored by the U. S. Atomic Energy Commission under contract with Union Carbide Corporation.

MASTER

DISTRIBUTION OF THIS DOCUMENT IS UNLIMITED

G-matrix used in the many-body theory of nuclear structure, although it is not very different (for qualitative purposes) from the simple potentials which fit low energy nucleon-nucleon scattering. The first term alone (which is closely related to a Hartree-Fock potential) gives a good account of the real part of the optical potential, as is illustrated in Fig. 1 for the scattering of 30 MeV protons [1]. This term, with the exchange neglected and v treated somewhat phenomenologically, is the basis of the so-called reformulated optical model of Greenlees, et al. [2]. This has been used to extract information about the density distribution $\rho(r_i)$ from analyses of elastic scattering data; however, the neglect of exchange and the higher order terms, as well as our lack of very accurate knowledge of the effective v , place limits on the accuracy of this procedure. One should not draw too strong conclusions about small effects such as differences between the proton and neutron distributions in the target.

The second and higher order terms give rise to the imaginary part of the potential (as well as contributing to the real part); so far only tentative calculations of these have been made.

Because v is spin and isospin dependent, so is the potential U . Further, because of the exchange and higher order terms, and any non-locality and energy dependence in v itself, U is both energy dependent and non-local. That is,

$$U_E \psi(\vec{r}) = \int U_E(\vec{r}, \vec{r}') \psi(\vec{r}') d\vec{r}'. \quad (2)$$

When we use a simple local potential as a model for U_E , this non-locality translates into additional energy dependence. Indeed, there is no reason

why the local model potential which is equivalent to U_E should be exactly the same for all partial waves; it may be L -dependent also. The energy dependence implied by the exchange terms in (1) agrees with that found phenomenologically for the real part of the potential from the scattering of protons of, say, 20 to 60 MeV [3].

Knowing the "true" U_E to be non-local, simple model potentials which are non-local have been introduced [4], especially of the form

$$U(\vec{r}, \vec{r}') = V(|\vec{r} + \vec{r}'|) H(|\vec{r} - \vec{r}'|), \quad (3)$$

in which all the observed energy dependence is thrown into the non-locality. Although very successful, this form is, of course, an oversimplification. Also it was soon realized that the scattering from such a potential could always be reproduced by an energy dependent local potential which is much easier to calculate with, and there is no advantage in using the non-local model for analysis of data. (Of course, the non-local models led to some interesting results, such as the relationship between the wavefunctions from local and non-local potentials [5].)

When the target density ρ is deformed or undergoes shape oscillations, the potential U can be expected to follow, and this generalization of the optical model to include non-spherical potentials allows one to calculate the direct component of inelastic scattering as well as understand the splitting of the s -wave strength function peak for deformed nuclei [6]. In light nuclei and at low energies (say up to a few MeV), the coupling between the various collective states in this generalized optical model can result in resonance-like behavior [6].

In the rest of this paper we shall review recent applications of

the optical model (the local version, except in one case) to various measurements involving neutrons.

In the context of optical model analyses, although it is clear that the optical model works very well in a qualitative sense, we might remark that many fits to the data are rather poor. Much of this we suspect is due to the low quality of the data. In particular most of the neutron scattering data are inadequate to determine precisely the features of the optical potentials; much better data are needed to be of such use in optical model analyses. (A lot of the proton data are, unfortunately, open to the same criticism. However, the very complete, precise and extensive set of scattering data for 30 MeV protons obtained at the Harwell PIA [7] represent an ideal in this respect.) There is also great interest in comparing neutron and proton optical model potentials [8]. Here we encounter further difficulties since data for the two nucleons tend to be available only for different regions of energy and target nuclei. Neutron data tend to be available at energies of 14 MeV and below 8 MeV, while the most useful sets of proton measurements are at 30 MeV and above. In addition many neutron measurements, especially on the heavier nuclei, sometimes do not completely resolve the first excited state. Proton data tend to be for the lighter nuclei ($A \leq 100$) (plus Pb!). It would really be valuable to have some good neutron scattering measurements at, say, 30 MeV.

2. Total Cross Sections

The work of Foster and Glasgow [9] must be mentioned. Total cross sections were measured from 2.5 to 15 MeV for 78 natural and 14 artificial or enriched elements from H to Pu. Figure 2 shows a sample for Ca through

Y and Fig. 3 shows Sn through Lu. The curves in these figures are the predictions from the non-local potential model of Perey and Buck [4], which has the form (3), using their original set of parameters (the same set for all nuclei). The agreement with the data is remarkable, particularly for the nuclei normally regarded as spherical. Some deviations begin to show in the middle of the energy range for nuclei heavier than Sn developing into large deviations for the deformed rare earths, which then die away again as one approaches the doubly magic Pb. Similar deviations show up for Th, U and Pu, and it is natural to associate them with collective vibrational and rotational effects. The measurements for the heavier elements ($A \gtrsim 200$) also exceed the predictions at the lowest energies.

The overall agreement with the Perey-Buck potential is evidence for the general validity of the concept of a universal optical model (as we remarked earlier, the fact that this happens to be a non-local potential is irrelevant; a local potential with the same number of parameters would do as well). The agreement over such a wide range of nuclei is probably due to the relative insensitivity of total cross sections to parameter changes provided some overall features are correct. The latter was guaranteed, apparently, by the original fitting procedure used by Perey and Buck [4] to determine their parameters. However, we would be surprised if the potential really was the same for all nuclei (except for scaling radii like $A^{1/3}$), and evidence that this is not so is provided by some 14 MeV total cross sections measured at Leningrad [10] (Fig. 4) which can be explained with a local potential by introducing a dependence of the strengths on the target symmetry parameter $(N-Z)/A$. (The other parameters, $r_0 = 1.26$ fm, $a = 0.70$ fm, $b = 1.0$ fm and $V_{s0} = 8.3$ MeV, are

similar to those of the local potential equivalent to the Perey-Buck potential.) To put these results in perspective, Fig. 5 shows the overall behavior of σ_T , with the slopes for the isotopes of Ni, Zn and Sn being indicated; the slopes for Ni and Zn are markedly different from the average trend. The symmetry dependence deduced for the real strength V is less than usually found for protons, but that for the imaginary part W is stronger [8,11].

Figure 6 shows measured σ_T for neutron energies up to 135 MeV for Cd and Pb [12] and for ^{165}Ho [13]. The oscillations with energy are clear evidence of the partial transparency of these nuclei to neutrons and have been understood in terms of a nuclear Ramsauer effect [14]. The data above 10 MeV for Cd and Pb were fitted with a local and spherical optical potential, corresponding to the dashed curves shown. (The predictions for this potential below 10 MeV are also shown; the deviation from experiment for Pb at the lowest energies is similar to that found with the Perey-Buck non-local potential.) This potential has both volume and surface absorption terms and depends linearly on the energy. The parameters are $V = (47.30 - 0.227 E_n) \text{ MeV}$, $W = (0.46 + 0.11 E_n) \text{ MeV}$, $W_D = (4.3 - 0.041 E_n) \text{ MeV}$, and $V_{SO} = 7.0 \text{ MeV}$ with $r_0 = r'_0 = 1.21 \text{ fm}$, $a = 0.68 \text{ fm}$ and $a' = 0.645 \text{ fm}$. The surface absorption term vanishes for $E_n \approx 105 \text{ MeV}$. The behavior with energy is similar to that observed for protons [11].

The dashed curve does not give a good fit to the strongly deformed ^{165}Ho . However, considerable improvement is obtained [13] when Ho is treated as a rigid rotor by using the generalized, non-spherical optical potential in a coupled equations calculation [6]; this yields the solid curve. The optical parameters were taken to be the same as for the

spherical nuclei Cd and Pb (except for the usual 20% reduction in W and W_D to compensate for the explicit coupling to the rotational states which is now included [6]), together with a quadrupole deformation parameter $\beta = 0.33$. This is not an optimum fit since no parameters were adjusted; these calculations take too long for any extensive variation of parameters to be studied. However, comparison between the dashed and full curves makes it clear that the deformation effect is important and improves agreement with the data.

The σ_T for ^{165}Ho were also measured [13] when the target nuclei were oriented at low temperatures. When non-spherical nuclei are oriented with respect to the direction of the incident neutrons, the average path length to traverse the nucleus is changed from what it is when the nuclei are randomly oriented. As a consequence the oscillations in σ_T with energy due to the Ramsauer effect are shifted. Figure 7 shows the change in σ_T versus E_n . The non-spherical optical potential (solid curve) reproduces this deformation shift very well. (The dashed curve comes from an approximate treatment [13] of this effect, using geometric optics and a square well potential [14].)

3. Elastic Scattering

Becchetti and Greenlees [15] reported on a global fit to 30 sets of neutron data from Fe to Pb for neutron energies below 15 MeV (except for 3 cases at 24 MeV). The parametrization of the potentials which they used is based on their proton analysis and included dependence on both energy and symmetry parameters $(N-Z)/A$. Few of the parameters were determined from the neutron data, the others being fixed at the values

obtained from their proton study. This bias is unfortunate because the proton analysis was strongly influenced by the extensive data for energies of 30 and 40 MeV, much higher than the neutron energies. The geometrical parameters they used are significantly different from those normally obtained from analyses of neutron data at these low energies (see below). Consequently it is not clear to which extent the results they obtained are biased to compensate for this effect. The fits which they obtained were reasonable but the compound elastic scattering was adjusted to obtain a best fit and this further complicates an assessment of their results. One of the less successful aspects of their analysis is the failure to reproduce adequately the total and reaction cross sections.

A very extensive study has been made by Holmqvist and Wedling [16] who have measured elastic differential cross sections for many elements from Al to Bi at energies from 1.5 to 8 MeV and have subjected the results to an optical model analysis. Figure 8 shows examples for Co and Cu; the fits are good. The optical model parameters are seen to be quite steady with energy (note the displaced zeros on the ordinate scales) and this provides further evidence for the validity of the model. Figure 9 shows the results for 22 elements at 8 MeV; again the fit is very satisfactory. We see from Fig. 10 that these optimum parameters (open circles) do not vary strongly with A ; the biggest fluctuations occur in the absorptive strength W , to which the fits are perhaps least sensitive. (Note again the displaced zeros on the scales.) The filled circles represent optimum values of V and W when the other parameters are fixed at the average values $r_0 = 1.22$ fm, $a = 0.67$ fm and $r'_0 = 1.23$ fm. ($V_{s0} = 8$ MeV and $a' = 0.48$ fm were fixed in all the studies.) The fluctuations in W remain, but those in V are reduced because they are correlated with the fluctuations in the radius r_0 and surface diffuseness a .

There is a general trend for V to decrease as A increases and this may be interpreted as a dependence on the neutron excess, or $(N-Z)/A$. The V and W are plotted against this symmetry parameter in Fig. 11. The trend is fairly clear for V , although there is considerable scatter. When it is expressed as $V = V_0 - V_1(N-Z)/A$, a least-squares fit is quoted as giving $V_1 \approx 12.5 \pm 2.5$ MeV. This value of V_1 is only about one-half that expected from analyses of proton scattering [8,11,15]. It has been emphasized by Greenlees, et al. that Eq. (1) suggests that a more significant measure of the real potential is the volume integral per particle, J/A , and this is also shown in Fig. 11. (One should not take too simple a view of J/A because of the effects of exchange and the higher order terms. Even without these, J/A will no longer be constant if the effective interaction v has any significant density dependence.) Because of the diffuse surface and the assumption that the radius is proportional to $A^{1/3}$, J/A decreases more rapidly than V as A (and hence, on average, $(N-Z)/A$) increases. The behavior in Fig. 11 is something like

$$J/A \approx 480 - 470 (N-Z)/A,$$

so the symmetry dependence is about twice as strong as expected from the simple Greenlees model. On the other hand, it is amusing to note that the J/A for 30 MeV protons shows no variation with $(N-Z)/A$ because in this case the variation of V is of opposite sign to that for neutrons and is just cancelled by the diffuse surface effect! We return to these features later.

The mean square radii of these neutron potentials are very close to those found from proton scattering. The other noticeable feature is that the average potential (which gives fits almost as good as those shown

in Figs. 8 and 9) has no energy dependence. However, we feel that an energy dependence of the usual magnitude in V and W (e.g., $\partial V/\partial E \approx -0.3$, or a change in V of about 2 MeV or 4% over the range $E_n = 1.5$ to 8 MeV) would probably give just as good fits. One should also remember that compound elastic corrections are made for the lower energies and this introduces some uncertainty.

We already saw that the non-spherical potential associated with a deformed nucleus affected the total cross section (Fig. 6). Figure 12 illustrates the effects on the elastic angular distributions for Ta [17]. The dashed curves show the best fits obtained with a spherical potential by varying five parameters at each energy. The solid curves results from coupled-channel calculations using a non-spherical potential with quadrupole deformations $\beta = 0.26$ and varying only two parameters, V and W , at each energy. The improvement in fit is dramatic. Rather similar results have been obtained for neutrons of 1.5 to 3.5 MeV on Er [18].

4. Inelastic Scattering

The generalized non-spherical optical potential allows one to calculate inelastic as well as elastic scattering [6], both to rotational or vibrational states. We mention the octupole state in ^{208}Pb as an example of the latter, taken from a recent evaluation of neutron data for Pb [19]. Figure 13 summarizes the elastic data used to determine the optical potential parameters (these are almost the same as the local equivalent to the Perey-Buck potential [4]). The left side of Fig. 14 shows the direct interaction fits to the excitation of the 2.6 MeV 3^- state (and also the 4.1 MeV group of states). Only the deformation parameter β is an adjustable parameter here, and the cross section is

proportional to β^2 (in the DWBA). Further, the β value must be compatible with values obtained from other measurements such as Coulomb excitation. Compound inelastic is negligible at these energies. However, at the lower energies shown on the right, the compound inelastic (calculated with the Hauser-Feshbach theory) dominates. Nonetheless, the direct contribution is not negligible for the 3^- even here; the dashed curves are from the compound process alone, while the solid curves include the direct excitation.

A corresponding analysis has been made for scattering from ^{56}Fe [20] for energies of 4 to 8 MeV. Figure 15 shows as a function of energy the percentage contribution from direct interaction for exciting the 2^+ state at 0.846 MeV. The quadrupole deformation parameter $\beta = 0.26$ was taken from an analysis of 11 MeV proton scattering so there were no adjustable parameters. Figure 16 compares the corresponding theoretical cross sections with the data; at 5 and 7.5 MeV, the direct (DI) and compound (CN) contributions are also shown separately.

The optical model, of course, plays an important role in providing transmission coefficients for Hauser-Feshbach calculations of compound inelastic scattering, but it does not seem appropriate to discuss these in detail here.

5. Isospin Dependence and (p,n) Reactions

We have already remarked upon the possibility of a dependence of the optical potential on the neutron excess or symmetry parameter $(N-Z)/A$. This is expected from the isospin dependence of the nucleon-nucleon force [8] and would have the opposite sign for neutrons and protons. If the symmetry potential is assumed to have the same shape as the main potential,

we might then expect well depths behaving like

$$V = V_0 \pm V_1 (N-Z)/A, W = W_0 \pm W_1 (N-Z)/A \quad (4a)$$

with + for protons, - for neutrons. A comparison of neutron and proton scattering would be the most direct way of extracting the parameters V_1 and W_1 but unfortunately few useful data are available for which the neutron and proton energies are similar. We then have to rely upon the variation of the potential for a given particle over a range of targets. Proton scattering data generally show this behavior [8,11,15] with $V_1 \approx 25$ MeV and $W_1 \approx 12$ to 16 MeV (for the surface absorption). (Of course, the precise values of V_1 and W_1 are meaningless unless we also specify the radius and surface diffuseness. However, we can ignore this for the qualitative comparisons we make here.) Neutron results are less clear-cut [8]. We have already seen (Fig. 4) σ_T measurements for a series of isotopes which were taken to imply $V_1 \approx 17$ MeV and $W_1 \approx 26$ MeV. The Swedish elastic scattering data have been taken to indicate (Fig. 11) $V_1 \approx 12.5 \pm 2.5$, with no clear variation in W . Unpublished analyses of 14 MeV data by one of us (FGP) are consistent with $V_1 \approx 0$. Hence there seem to be indications that V_1 is smaller for neutrons than for protons.

This situation changes if we take the view that the volume integral per particle is the more significant measure of the real potential. Because of the effect of the diffuse surface, even if V were constant then J/A would decrease with increasing A and, because $(N-Z)/A$ also tends to increase with A , J/A would appear to decrease with increasing neutron excess. Figure 11 illustrates this behavior for neutrons. For protons, on the other hand, this effect reduces the apparent symmetry dependence; at 30 MeV [7], J/A appears to be independent of $(N-Z)$. It has been

suggested [21] that if the nucleon-nucleon effective interaction v in Eq. (1) were density dependent (which it certainly is, to some extent), then this would also lead to a reduction in J/A as A increases, thus obscuring any dependence on neutron excess. Certainly this would help restore the symmetry between protons and neutrons. In addition, of course, there are other corrections to the first order term in Eq. (1), and these can be expected not to be exactly symmetric.

Hence our knowledge of the symmetry potential from elastic scattering remains uncertain, even though in general the differences $V_p - V_n$ or $(J_p - J_n)/A$ are of the order of magnitude expected. Another, more direct, measure of this potential becomes available if the suggestion of Lane [8] is adopted. The optical potential is written in the isospin form

$$U(r) = U_0(r) + 4 U_1(r) \vec{t} \cdot \vec{T} / A \quad (4b)$$

and hence immediately includes the (p,n) charge-exchange reaction which excites the analogue of the target ground state. The cross section for this then depends upon U_1 alone, instead of U_1 providing a small correction to the main interaction as in elastic scattering. There are now many experiments of this type [8]. We shall merely cite some recent evidence that $U_1(r)$ is complex, that it is energy-dependent and that it may contain a spin-orbit term.

Figure 17 shows some typical results at about 19 MeV from the old cyclotron at Livermore [22]. The curves are the predictions obtained using the $(N-Z)/A$ terms from the Becchetti-Greenlees [15] proton optical potential and assuming these truly represent $U_1(r)$; there are no adjustable parameters. The agreement is good. Including the imaginary terms here is important for giving the structure observed in the angular

distributions, so this represents evidence that U_1 is complex. This is illustrated further in the left side of Fig. 18 for a higher energy [23] and for a similar potential [11]. In this case the predicted cross section is too large. (The right side of Fig. 18 indicates the additional effect of having the real part of U_1 peaked at the surface instead of spread throughout the volume.)

Figure 19 tells a less comforting story. These measurements [24], at 23 MeV, are more precise and show that the observed angular distributions have more structure than is predicted by the Becchetti-Greenlees (curves) or similar potentials, although the overall magnitudes are quite close. We do not know whether taking the real part of U_1 to be surface peaked would improve the agreement, but it seems likely. Carlson, et al. [24] chose to vary the imaginary part of U_1 in such a way as to emphasize the contributions from the surface region and found a form which fitted the (p,n) as well as the corresponding (p,p) and (n,n) distributions in a self-consistent way (Fig. 20). The shapes of the real (dashed curves) and imaginary (full curves) parts of $U_1(r)$ are shown in Fig. 21. The real part has the same shape as in the Becchetti-Greenlees potential except for a reduction in strength of 20 to 30%, but the imaginary part is very different. Its radius remains almost constant but its width increases as A increases. We find such a potential hard to understand.

In passing, we note that Fig. 19 shows a marked difference between ^{26}Mg with $I = 0$ and ^{25}Mg and ^{27}Al , both with $I = 5/2$. This may be evidence for a deformed U_1 whose non-spherical components can contribute in lowest order to the latter two targets but not for the former.

We turn next to the energy dependence of U_1 . Elastic scattering data have been consistent with $U_1 = \text{constant}$, independent of energy.

Recent measurements at UCLA [25] of the total $(p, \tilde{n}p)$ cross section reveal an energy dependence quite different from that predicted for a constant $U_1(r)$; Fig. 22 shows two examples. Curves (a) are for U_1 from the Becchetti-Greenlees potential, assuming 100% \tilde{p} -decay of the analog state. Apparently there is a discrepancy between the absolute magnitudes of $\sigma_T(\tilde{p})$ and $\sigma_T(p, n)$ which is not understood at present, but the energy dependence is believed to be valid. Supporting evidence comes from the new Livermore cyclograaff [26], Fig. 23, which also shows an energy dependence much stronger than predicted by the optical model, as well as a larger cross section at the lower energies. It has been suggested [25] that these effects would be explained by solving exactly the coupled neutron-proton equations instead of using the DWBA, but we find this hard to believe. On the other hand, we have no better explanation to offer.

Finally we mention recent measurements at Saclay on these (p, n) reactions using polarized protons of 25 MeV [27]. It appears to be difficult to fit the asymmetry for forward scattering angles without including a spin-orbit term in U_1 . (This is rather reminiscent of asymmetry measurements on (p, p') , where the results for small angles require a spin-orbit component in the deformed optical potential.) Figure 24 shows an example, where the spin-orbit strength is also written like Eq. (4),

$$V_S = V_{SO} \pm V_{S1} (N-Z)/A.$$

The sign of V_{S1} is negative, as expected from the nucleon-nucleon spin-orbit force. Now $V_{S1} = -1$ MeV implies a spin-orbit strength for protons on Pb which is only about 7% weaker than for neutrons. This small difference could hardly be detected in analyses of elastic scattering. More experiments of this type would be useful.

6. Spin-Spin Interactions

A number of attempts have been made to detect the effects on nucleon-nucleus scattering of a coupling between the spin $\frac{1}{2} \vec{\sigma}$ of the nucleon and the spin \vec{I} of the target. This coupling is usually discussed in terms of a potential of the form

$$U_{ss}(r) \vec{\sigma} \cdot \vec{I} \quad (5)$$

although in general this is only one of several possible forms [28]. We may have scalar products of other tensors, for example

$$U = \sum_{LJ,M} a_{LJ}(r) (-)^M T_{J,M}(\vec{I}) T_{LJ,-M}(\theta, \phi, \vec{\sigma}). \quad (6)$$

Here L is even, and $L = J$ or $J \pm 1$. The rank J is restricted by the target spin to be $J \leq 2I$. The form (5) follows from $L = 0, J = 1$. The values $L = 2, J = 1$ give the next simplest term,

$$U_T(r) [3(\vec{\sigma} \cdot \hat{r})(\vec{I} \cdot \hat{r}) - \vec{\sigma} \cdot \vec{I}], \quad (7)$$

which is like the usual tensor force.

Comparisons of scattering from even, spin zero targets and odd targets with non-zero spin have shown no marked differences, indicating that spin-spin effects are not large. Clearly, however, the optimum way to search for such interactions is to scatter polarized nucleons from polarized targets and this has been done a number of times [29]. The most recently published work scatters polarized neutrons of 0.3 to 8 MeV from polarized ^{59}Co ; Fig. 25 shows the difference between the total cross sections measured when the two spins are aligned parallel and antiparallel,

$$\sigma_{ss} = (\sigma_{\uparrow\uparrow} - \sigma_{\uparrow\downarrow})/2 P_n P_t.$$

The curves are the predictions using a term like (5) when $U_{ss}(r)$ has a Woods-Saxon shape with a depth V_{ss}/I ; the theoretical predictions are rather insensitive to the shape chosen. No single value of V_{ss} will fit the data around 1 MeV. However there are appreciable fluctuations and intermediate structures in σ_T in this energy region (Fig. 26) which may account for these difficulties. There is also the possibility [30] of contributions from higher rank tensors such as (7).

The uncertainties summarized in Fig. 25 certainly make it desirable to have accurate measurements for higher neutron energies. Current development of sources of polarized neutrons resulting from polarization transfer reactions may make such measurements easier. At the same time it would be valuable to compare measurements in which the polarizations were parallel and perpendicular to the incident beam. The vector interaction (5) gives the same result in both geometries but the effect of the tensor term (7) changes sign [30].

The other popular target for these measurements is ^{165}Ho [31]; σ_T data have been taken at 0.4, 1, 8 and 15 MeV. The overall result is that the measurements are compatible with $V_{ss} = 0$, although values of several hundred KeV are allowed.

Another attempt to detect the spin-spin interaction is a measurement of the depolarization of 1.4 MeV polarized neutrons by a number of odd-A targets [32]. The depolarizations measured were quite large; unfortunately it appears they are largely due to compound elastic scattering rather than the direct intervention of a spin-spin potential.

Some theoretical estimates of the strength of the spin-spin interactions have been made [28,29]. These assume the model of Eq. (1), with the spin-spin term coming from the last odd nucleon of the target, and indicate that U_{ss} should be quite weak. Figure 27 shows an example for ^{59}Co [28]; the neutron potential is similar but of opposite sign. It was also noted that core polarization effects (the same that make the magnetic moment depart from the Schmidt value and which tend to inhibit M1 transitions) tend to quench the spin-spin interaction. The curve C is the contribution from the direct central force coupling to the valence nucleon, while CP is from the core polarization. Contributions from two choices of tensor force are also shown. These calculations suggest U_{ss} has a strength of less than 100 KeV. Similar calculations of the tensor term (7) indicate that this is weak also.

7. Strength Functions

The theoretical background to strength functions and their relation to the optical model have been reviewed in several places recently [33]. It is our impression that there have not been many striking developments in this subject in the last few years. Some of the old puzzles remain with us, only partially understood; e.g., the very low minima in S_0 near $A \sim 100$ (Fig. 28) and in S_1 near $A \sim 50$ and $A \sim 170$. The s-wave minimum was explained by Moldauer [34] as due to the imaginary part of the optical potential being concentrated in a narrow shell at a radius about 0.5 fm greater than the real potential (curve 5 in Fig. 28). It is interesting that a similar conclusion is reached from absorption cross section measurements for low energy (3 to 5 MeV) protons on the Sn isotopes [35]. However, we find it difficult to understand such a localized absorption,

and we tend to believe this is merely a device to reduce the s-wave absorption for the $A \sim 100$ region compared to other masses. There is no reason why the potential should not be somewhat different for s- and p-waves, or vary somewhat with A in a non-monotonic way [36].

Recent measurements at RPI [37] of the p-wave strength function show some very low values in the region of $A \sim 50$, much lower than predicted by Moldauer's potential. Further, it is still not clear experimentally whether the p-wave peak for $A \sim 100$ is split or not. S_1 does attain very high values for some targets in this region. It has been stressed [38] that this p-wave peak is related to the cusp seen in (d,p) excitation functions in the $A \sim 90$ region at the threshold for the analog (d,n) transition. The outgoing proton from the (d,p) reaction is coupled through the interaction (4b) to the neutron from the (d,n) reaction which is exciting the analog state of the residual nucleus. At the threshold for the latter, when $A \sim 90$ the zero-energy neutron is dominated by the $3p$ -wave "giant resonance". Then the observed cusp in the (d,p) excitation function reflects fairly directly the energy profile of the $3p$ strength function. (A simple description of this phenomenon has been given by Lane [39].)

The s-, p- and d-wave strengths for neutrons on ^{40}Ca with energies up to 2 MeV have been studied recently. The l and J of 71 resonances up to 1.5 MeV were identified and the results tied in with information for negative energies from the (d,p) reaction [40]. The p-wave resonances amount to only 1% of the single particle value \hbar^2/ma^2 , which is consistent with almost all the $2p$ strength being in the bound states, 5 to 7 MeV lower, which are populated by the (d,p) reaction. Further, the $p_{1/2}$ strength was greater than the $p_{3/2}$, as expected. Also in this energy

range, 7% of the Wigner limit was seen for s-waves, and 6% for d-waves, which again is consistent with the bulk of the 3s and 2d single particle strength being somewhat higher in excitation, as expected from a simple potential model.

Some d-wave strength functions have been extracted recently from capture cross section measurements for 12 elements from Nb to Au [41]. Agreement with the predictions of a spherical optical potential was not very good, but this is not too surprising since several targets were from the deformed rare earth region and others exhibit quite strong quadrupole vibrations. This work also contributes some more low p-wave strength functions for the rare earths and some high ones for the $A \sim 100$ region.

Another possibility for obtaining information about d-wave neutrons is to study inelastic excitation of the first 2^+ level near threshold. Then only s-wave outgoing neutrons contribute and therefore angular momentum conservation selects incoming d-waves.

Values of S_0 for a number of isotopic series were deduced at Saclay [42] recently from measurements of parameters of individual resonances. They show (Fig. 29) a strong dependence on neutron excess, very different from the predictions (solid curve) of an optical potential with fixed parameters. Indeed, a very strong dependence of the absorptive potential W on $(N-Z)/A$ ($W_1 = 63$ MeV in Eq. (4a)) is required to reproduce this behavior. This is very similar to the σ_{π} behavior shown in Fig. 4, although the symmetry dependence needed there was not as strong. Apparently $W_1 = 45$ MeV gives agreement with the data for the Sn isotopes. It is interesting that analyses [43] of the elastic scattering of 16 MeV protons from these targets also resulted in a symmetry dependence, somewhat weaker

($W_1 \approx 44$ MeV for Te, $W_1 \approx 23$ MeV for Sn and Cd) but of the opposite sign, i.e., as expected for a true isovector potential of the form (4b). However the two effects, for such different energies, may be quite unrelated [36].

This same group [42] has measurements for some odd mass targets pertaining to a possible spin dependence of S_0 (which might be related to a spin-spin term in the optical potential). Unfortunately the results are rather inconclusive. For example, on ^{143}Nd , the ratio $S_0(J=4)/S_0(J=3) \approx \frac{1}{2}$, while for ^{145}Nd it is about 2.7. This ratio is also about 2 for ^{147}Sm and ^{149}Sm , but the two spin states for ^{123}Te and ^{125}Te targets have roughly equal strengths.

Finally, we should remark that a large amount of information on proton strength functions is being accumulated for the mass region $40 \leq A \leq 64$ at Duke, and this has been reviewed recently by Bilpuch [44].

8. Concluding Remarks

In conclusion, we would like to comment on the "richness" of the optical model concept and its applications. Besides being a device for correlating data, it acquires immediate physical significance through interpretations such as that underlying Eq. (1). The potential has been enriched through the inclusion of spin-orbit and spin-spin terms which enable polarization measurements to be described. The dependence of the potential on neutron excess can lead to interesting nuclear structure information; the generalization of this in the isospin language immediately includes a class of (p,n) reactions. Allowing the potential to be non-spherical (or to oscillate in shape about a spherical mean) immediately includes within the domain of the optical model a large class of inelastic scattering reactions. Finally, of course, these "optical" phenomena play an important role in the description of transfer and other reactions.

References

1. G. R. Satchler, *Comments on Nuclear & Particle Physics* 5, 39, 1972.
2. G. W. Greenlees, G. J. Pyle and Y. C. Tang, *Phys. Rev.* 171, 1115, 1968.
3. L. W. Owen and G. R. Satchler, *Phys. Rev. Lett.* 25, 1720, 1970.
4. See, for example, F. G. Perey and B. Buck, *Nucl. Phys.* 32, 353, 1962;
C. A. Engelbrecht and H. Fiedeldey, *Ann. Phys.* 42, 269, 1967.
5. N. Austern, *Phys. Rev.* 137, B752, 1965.
6. See, for example, T. Tamura, *Ann. Rev. Nucl. Science* 19, 99, 1969.
7. V. Hnizdo, et al., *Phys. Rev.* C3, 1560, 1971, and other references given there.
8. G. R. Satchler, in *Isospin in Nuclear Physics* (North-Holland Publishing Co., 1969) and references given there.
9. D. G. Foster and D. W. Glasgow, *Phys. Rev.* C3, 576 and 604, 1971.
10. Yu. K. Dukarevich, A. N. Dyumin and D. M. Kaminker, *Nucl. Phys.* A92, 433, 1967.
11. J. J. H. Menet, et al., *Phys. Rev.* C4, 1114, 1971.
12. P. H. Bowen, et al., *Nucl. Phys.* 22, 640, 1961.
13. H. Marshak, et al., *Phys. Rev.* C2, 1862, 1970.
14. J. M. Peterson, *Phys. Rev.* 125, 955, 1962.
15. F. D. Becchetti and G. W. Greenlees, *Phys. Rev.* 182, 1190, 1969.
16. B. Holmqvist and T. Wiedling, *Nucl. Phys.* A188, 24, 1972;
B. Holmqvist and T. Wiedling, *Neutron Physics Lab. (Studsvik) Report* AE-430, 1971;
B. Holmqvist and T. Wiedling, *Phys. Lett.* 26B, 620, 1972;
B. Holmqvist, *Ark. f. Fys.* 38, 403, 1968.
17. B. Holmqvist, et al., *Nucl. Phys.* A150, 105, 1970.

18. S. Tanaka, et al., Nucl. Phys. A179, 513, 1972.
19. C. Y. Fu and F. G. Perey, Oak Ridge National Laboratory Report ORNL-4765, 1972.
20. W. E. Kinney, Oak Ridge National Laboratory Report ORNL-TM-2052, 1968.
21. B. C. Sinha, Phys. Lett. 33B, 279, 1970.
22. C. Wong, et al., Phys. Rev. C5, 158, 1972.
23. C. J. Batty, et al., Nucl. Phys. A116, 643, 1968.
24. J. D. Carlson, D. A. Lind and C. D. Zafiratos, to be published.
25. T. J. Woods, G. J. Igo and C. A. Whitten, Phys. Lett. 39B, 193 1972;
G. W. Hoffmann, et al., Nucl. Phys. A187, 577, 1972 and to be published.
26. J. L. Anderson, private communication.
27. J. M. Moss, et al., to be published.
28. G. R. Satchler, Particles & Nuclei 1, 397, 1971.
29. T. R. Fisher, et al., Nucl. Phys. A179, 241, 1972 and other references given there.
30. T. R. Fisher, Phys. Lett. 35B, 573, 1971.
31. T. R. Fisher, D. C. Healey and J. S. McCarthy, Nucl. Phys. A130, 609, 1969 and other references given there.
32. K. Katori, et al., J. Phys. Soc. Japan 28, 1116, 1970.
33. See, for example, P. A. Moldauer, in Statistical Properties of Nuclei (Plenum Publishing Press, 1971);
J. E. Lynn, Neutron Resonance Reactions (Oxford University Press, 1968).
34. P. A. Moldauer, Nucl. Phys. 47, 65, 1963.
35. C. H. Johnson and R. L. Kerneil, Phys. Rev. C2, 639, 1970.
36. W. G. Vonach, A. B. Smith and P. A. Moldauer, Phys. Lett. 11, 331, 1964; B. Block and H. Feshbach, Ann. Phys. 23, 49, 1963; C. Shakin, Ann. Phys. 22, 373, 1963.

37. See, for example, H. W. Newson, in Statistical Properties of Nuclei (Plenum Publishing Press, 1971).
38. R. Coker and T. Tamura, Phys. Rev. 182, 1277, 1969.
39. A. M. Lane, Phys. Lett. 33B, 274, 1970.
40. J. Nebe and G. J. Kirouac, Nucl. Phys. A185, 113, 1972.
41. D. Kompe, Nucl. Phys. A133, 513, 1964.
42. B. Cauvin, et al., Annual Report 1970-71, CEN Saclay, CEA-N-1522;
H. Tellier and C. M. Newstead, Proc. Third Conf. on Neutron Cross Sections and Technology, Knoxville, 1971.
43. W. Makofske, et al., Phys. Rev. 174, 1429, 1968.
44. E. G. Bilpuch, in Statistical Properties of Nuclei (Plenum Publishing Press, 1971).

Figure Captions

Figure 1. Elastic scattering predicted for real potential based on first term of Eq. (1) plus phenomenological imaginary and spin-orbit terms [1] compared to measurements.

Figure 2. Total cross sections for elements from Ca to Y, from Ref. [9].

Figure 3. Total cross sections for elements from Sn to Lu, from Ref. [9].

Figure 4. Total cross sections for some isotopic sequences for 14 MeV neutrons [10]. Solid curves are experimental, dashed curves are optical model calculations.

Figure 5. Total and elastic cross sections for 14 MeV neutrons. Lines I, II and III indicate the trends from Ref. [10], Fig. 4.

Figure 6. Total cross sections for neutrons up to 135 MeV [12,13]. Dashed curves are for spherical optical potential, fitted to data above 10 MeV for Cd and Pb. Solid curve is for deformed, rotational optical model.

Figure 7. Deformation effect in total cross sections for neutrons up to 135 MeV on oriented ^{165}Ho [13]. Solid curve is deformed optical model prediction, dashed curve is for an approximate calculation.

Figure 8. Elastic differential cross sections for neutrons of 1.5 to 8 MeV on Co and Cu, with optical model fits [16]. Corresponding parameters for Cu shown on right.

Figure 9. Elastic scattering at 8 MeV from a series of targets, with optical model fits [16].

Figure 10. Optical potential parameters for Fig. 9. Solid dots are for two parameter (V and W) fits with other parameters fixed at the average values.

Figure 11. As Fig. 10, but plotted against neutron excess. JU/A is the

volume integral per nucleon for the real part of the potential.

Figure 12. Elastic scattering from Ta at energies from 2.5 to 8 MeV [17].

Dashed curves are best fits using spherical optical potentials; solid curves are for the non-spherical rotational model.

Figure 13. Summary of optical model fits to elastic scattering from Pb [19].

Figure 14. Vibrational optical model fits to inelastic scattering from Pb (left), together with compound inelastic calculations at lower energies (right) [19]. Difference between dashed and solid curves is the direct reaction contribution.

Figure 15. Variation with energy of direct (vibrational optical model) contribution to excitation of lowest 2^+ state in ^{56}Fe [20].

Figure 16. Differential cross sections corresponding to Fig. 15. Direct (DI) and compound (CN) parts shown separately at 5 and 7.55 MeV.

Figure 17. Excitation of the analog of the target ground state by (p,n) reaction at 18.7 (left) and 19.7 (right) MeV [22]. Curves are predictions from symmetry dependent parts of Becchetti-Greenlees potential.

Figure 18. Effect of complex isovector interaction on (p,n) angular distribution. Real part has Saxon ("volume") or derivative of Saxon ("surface") shape.

Figure 19. As Fig. 17, except at 23 MeV [24].

Figure 20. Simultaneous fits to (p,n) reaction at 23 MeV together with corresponding proton and neutron elastic scattering [24].

Figure 21. Isovector potentials used for calculations shown in Fig. 20; real parts are dashed, imaginary parts are solid curves.

Figure 22. Energy dependence of total cross section for (p,n̄) reaction [25]. Curves "a" are predictions using Becchetti-Greenlees potential.

Figure 23. Total cross section for $^{51}\text{V}(p,n)$ reaction [26].

Figure 24. Asymmetry from using polarized protons in $^{116}\text{Sn}(p,n)$ analog reaction [27]. Curves are optical model predictions with isovector spin-orbit term of strength V_{S1} added.

Figure 25. The spin-spin effect on the total cross section for polarized neutrons on polarized ^{59}Co [29]. The curves are optical model predictions with a term $V_{ss} \vec{I} \cdot \vec{\sigma} / I$.

Figure 26. As Fig. 25, but with fine resolution, between 0.3 and 1.8 MeV [29].

Figure 27. Calculated spin-spin potential for protons on ^{59}Co ; contributions from central (C), tensor (OPEP and TPEP) and core polarization (CP) forces [28].

Figure 28. Neutron S-wave strength function and optical model calculations [34].

Figure 29. Neutron S-wave strength function for Te isotopes and optical model calculations [42].

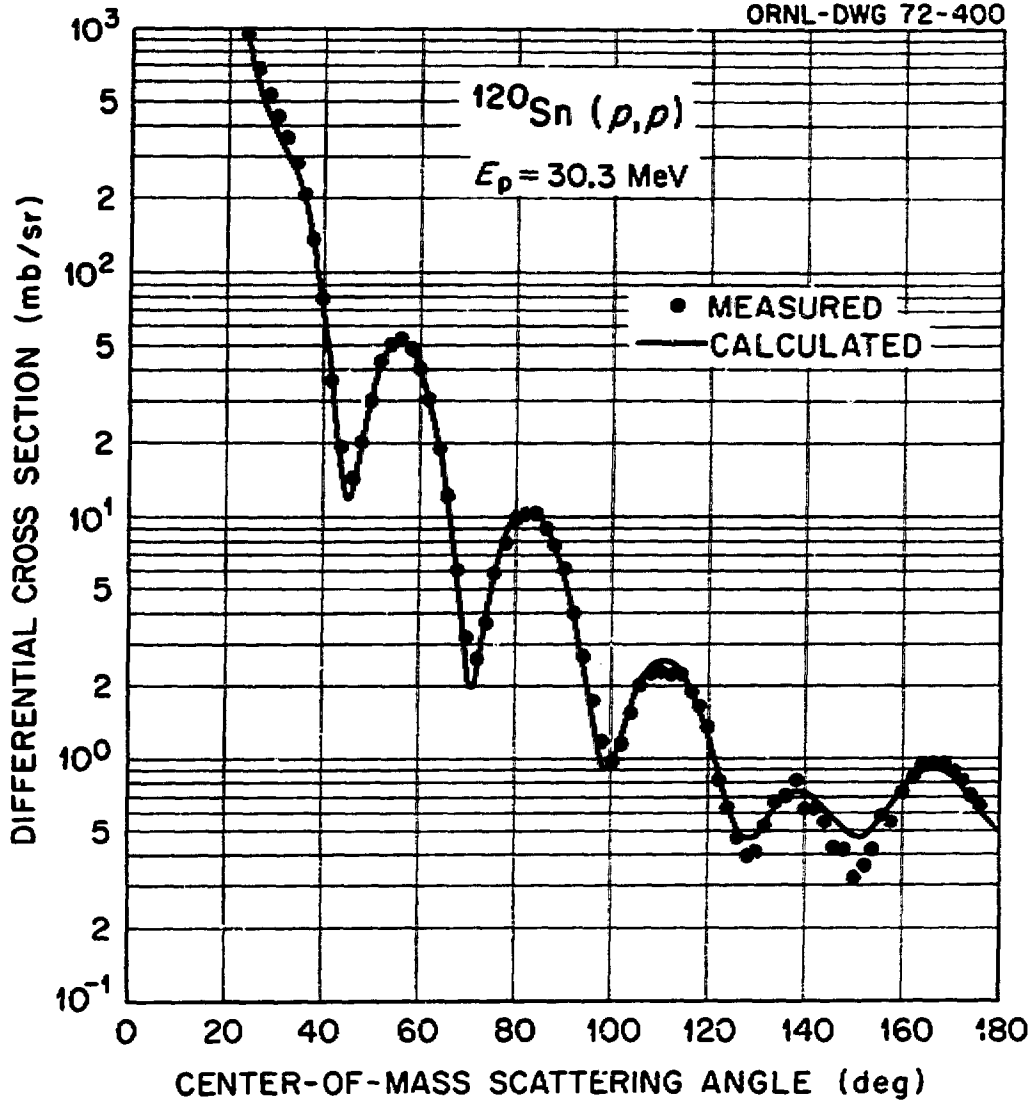


FIGURE 1

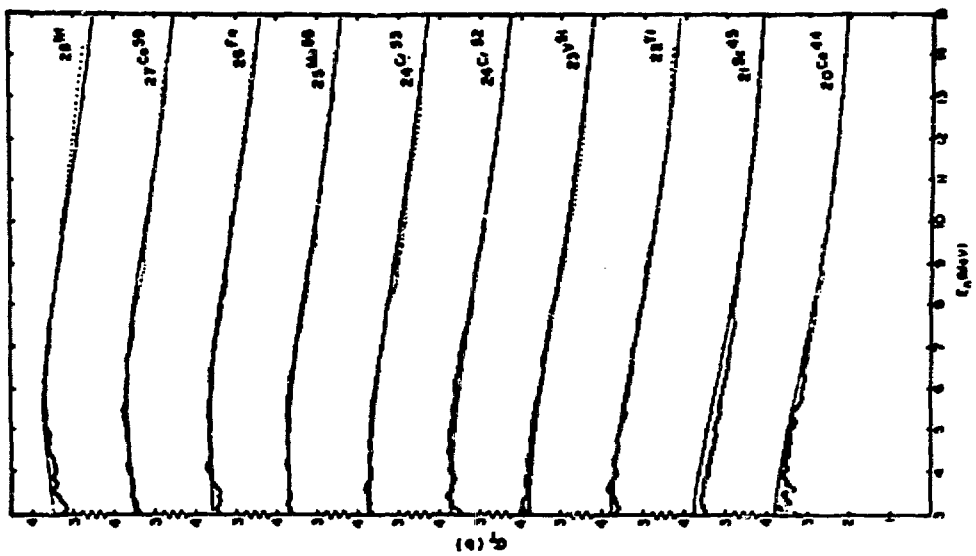
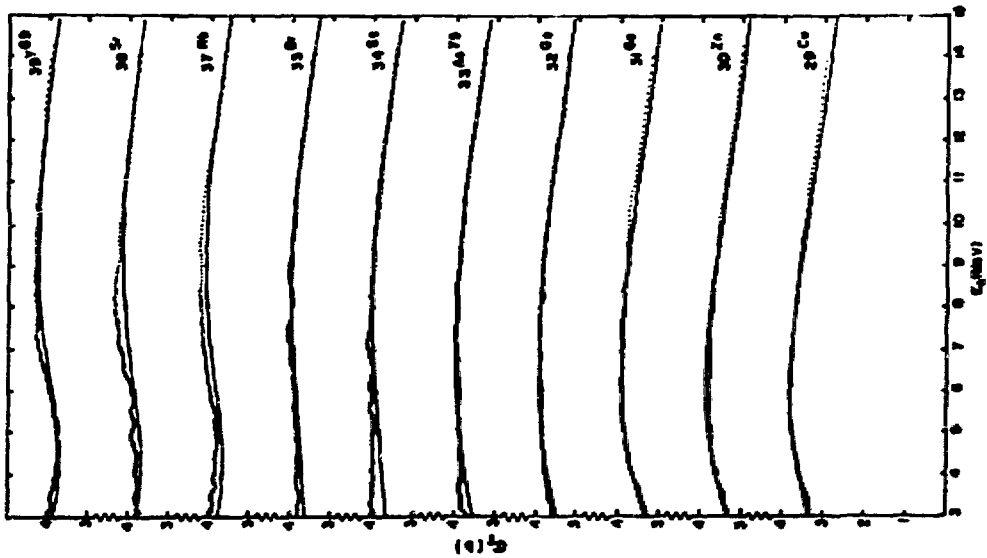


FIGURE 2

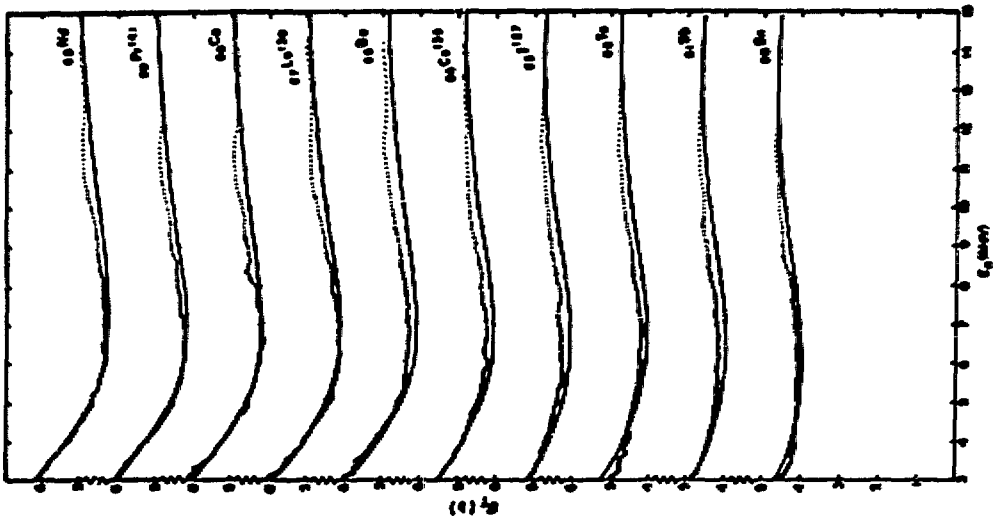
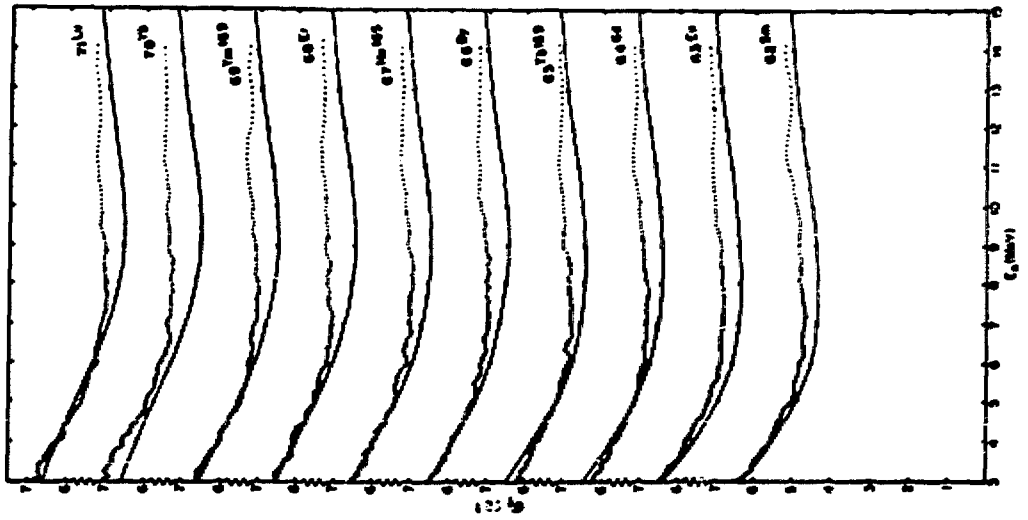


FIGURE 3

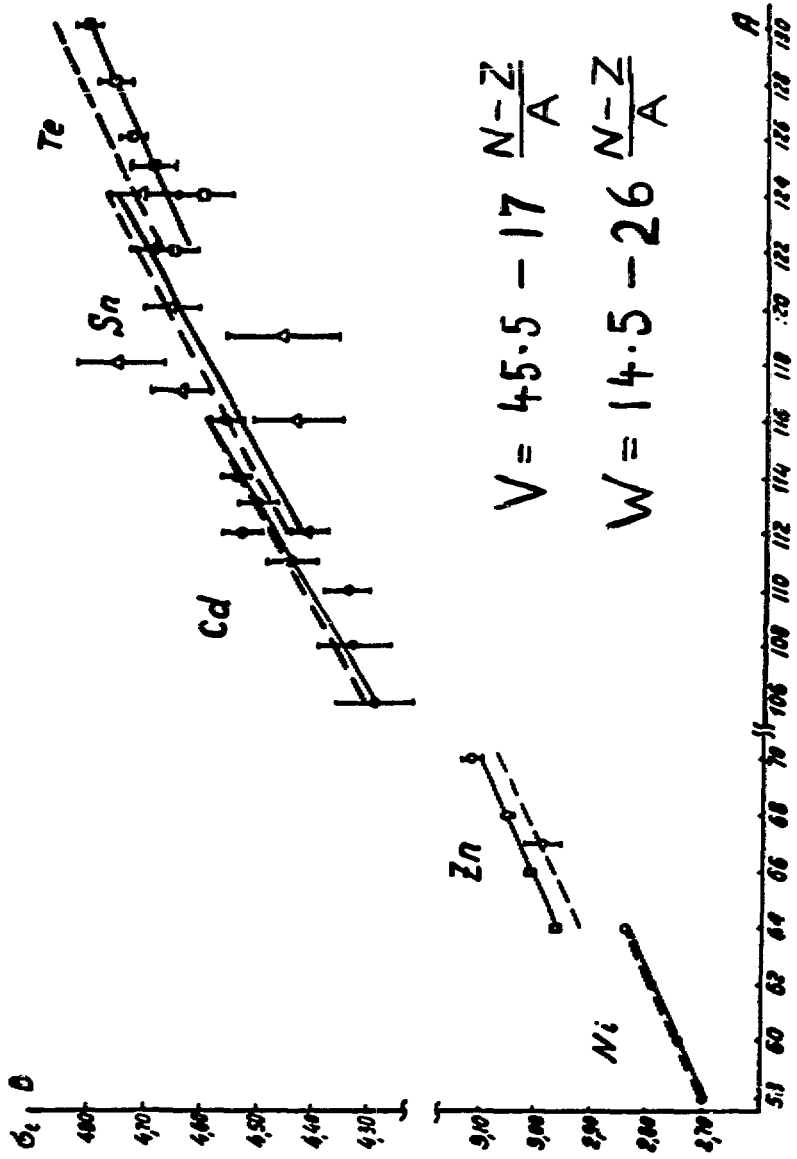


FIGURE 4

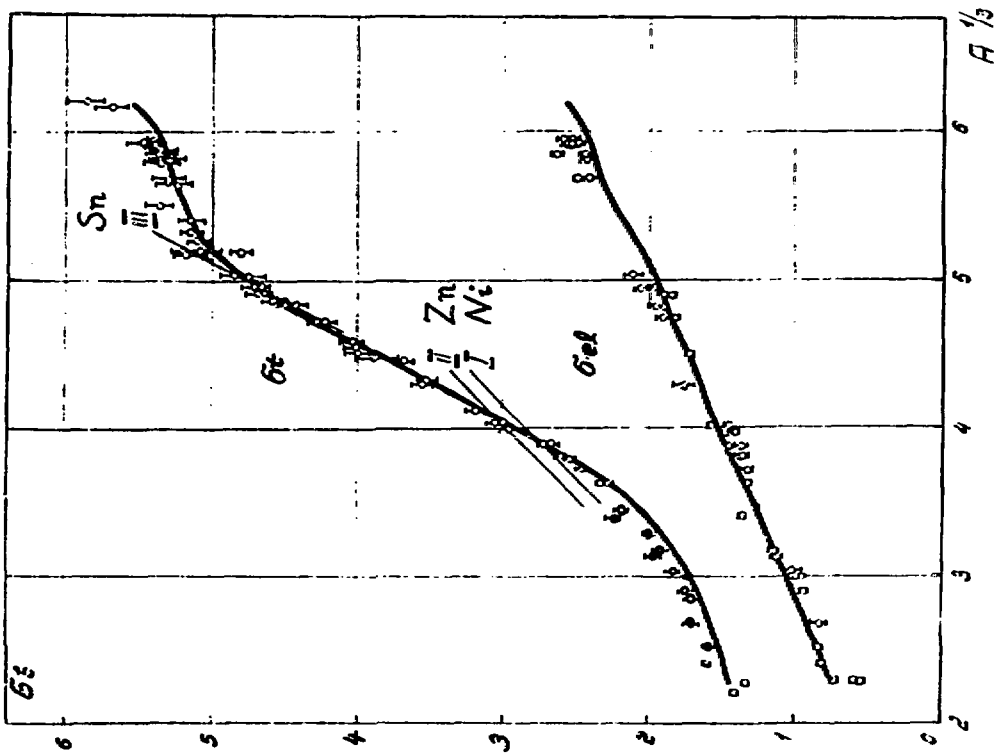


FIGURE 5

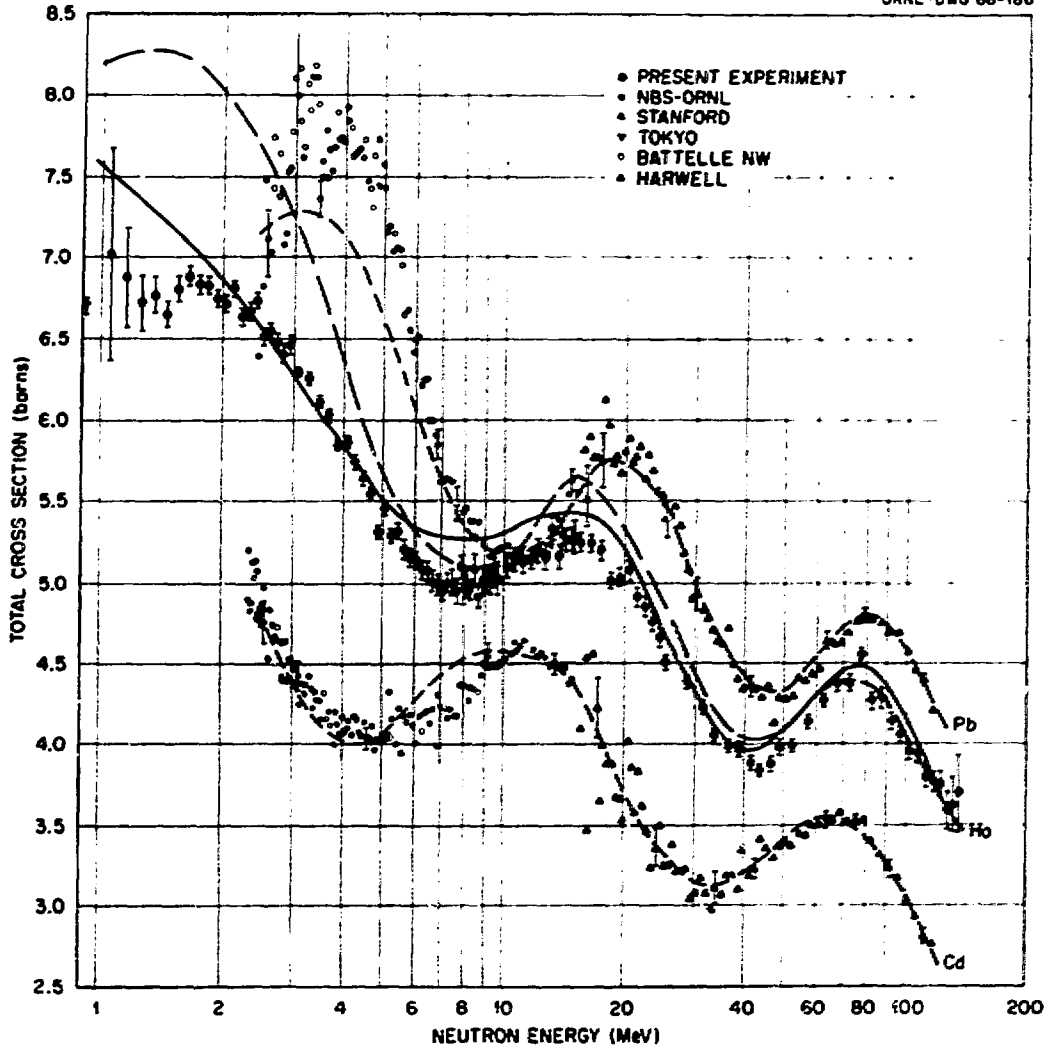


FIGURE 6

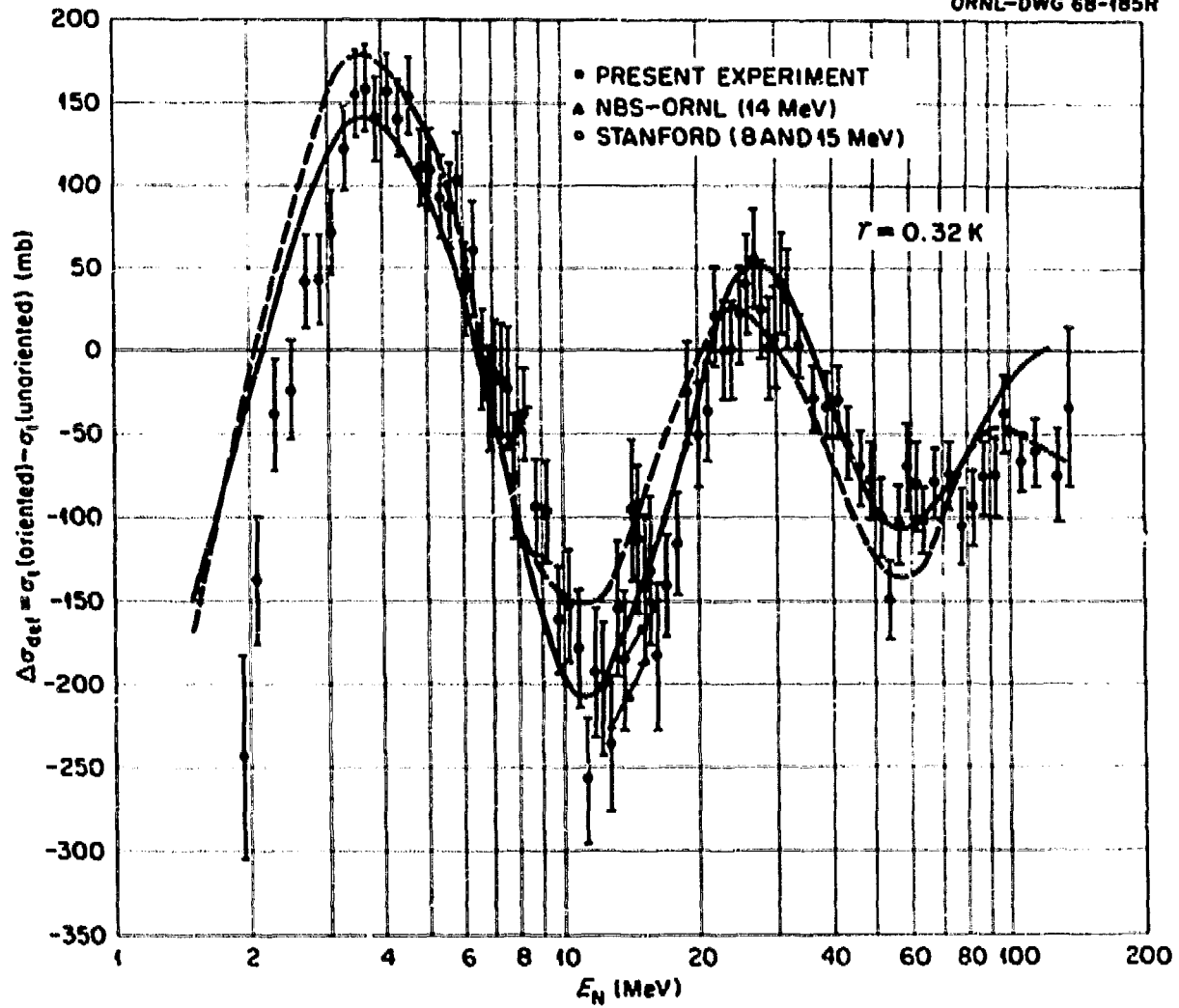


FIGURE 7

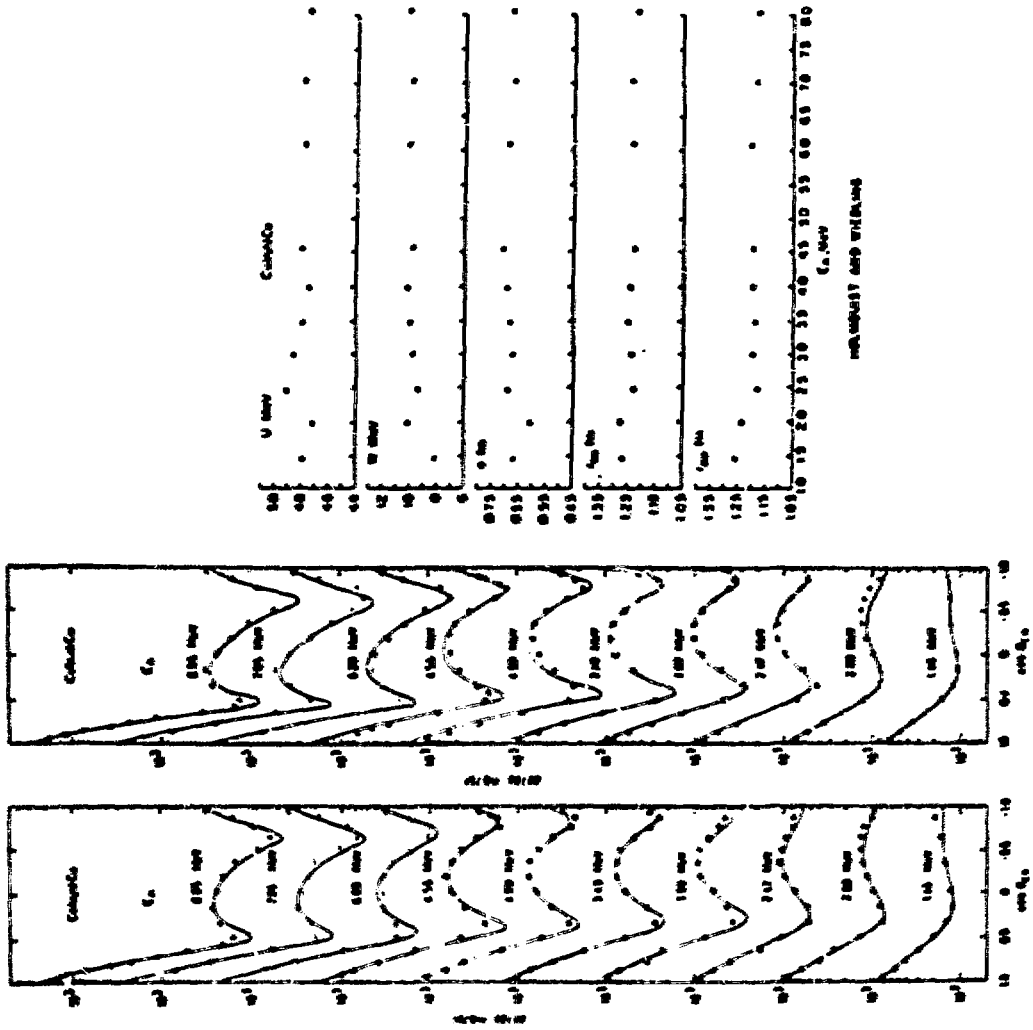


FIGURE 8

R. HOLMQUIST AND T. WIEDLING

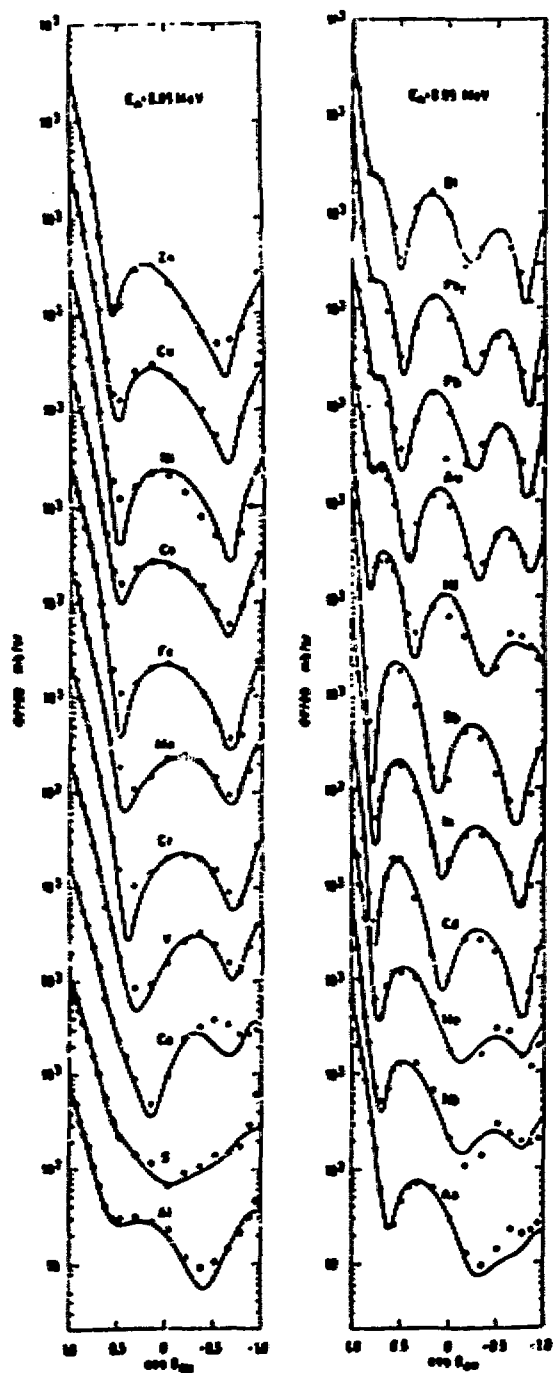


FIGURE 9

NEUTRON SCATTERING

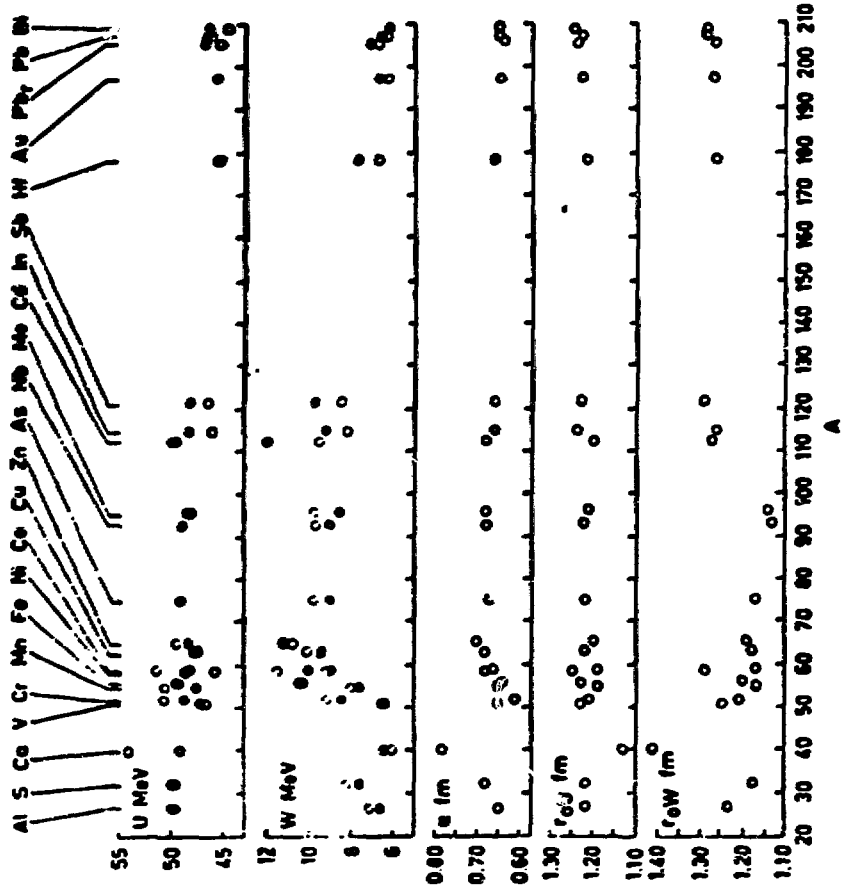
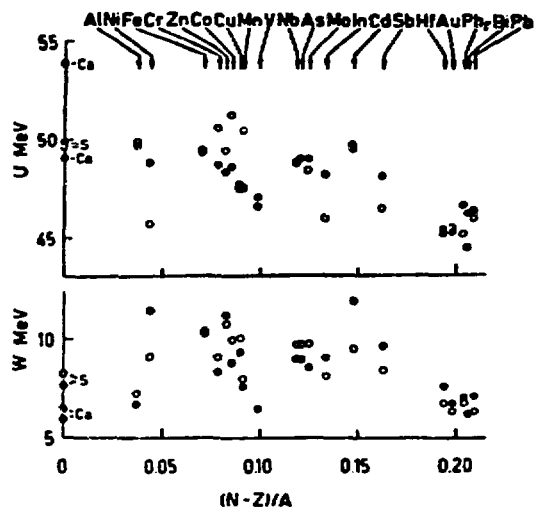
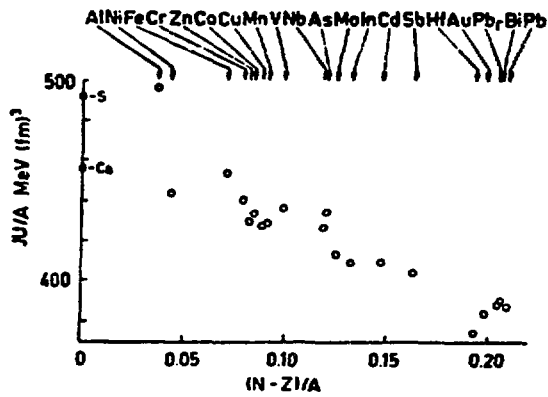


FIGURE 10



The optimum values of U and W from the two-parameter (filled circles) and five-parameter (circles) analyses plotted as functions of the symmetry parameter $(N-Z)/A$.



The quantity JU/A plotted as a function of the symmetry parameter $(N-Z)/A$.

FIGURE 11

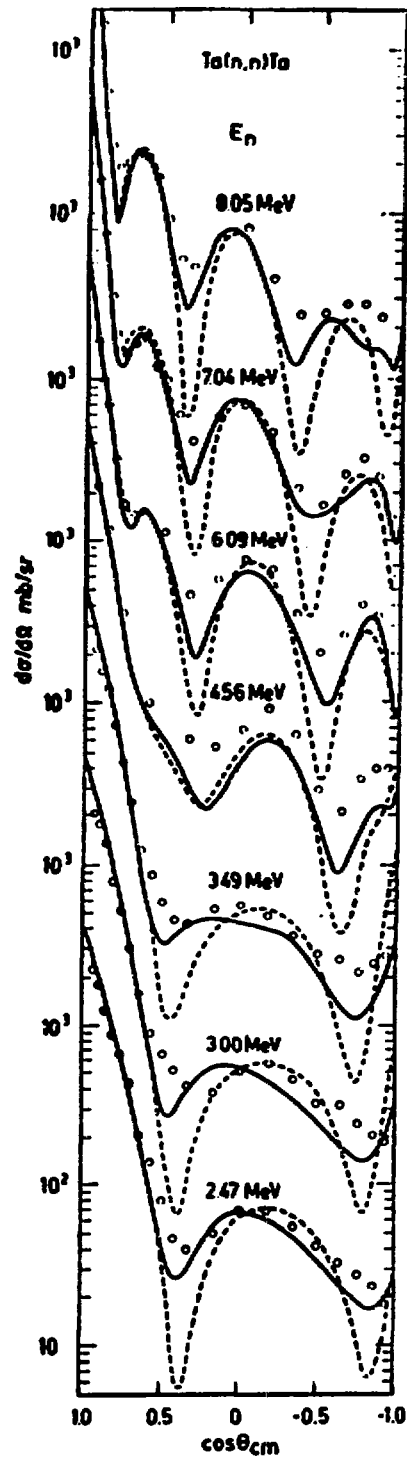


FIGURE 12

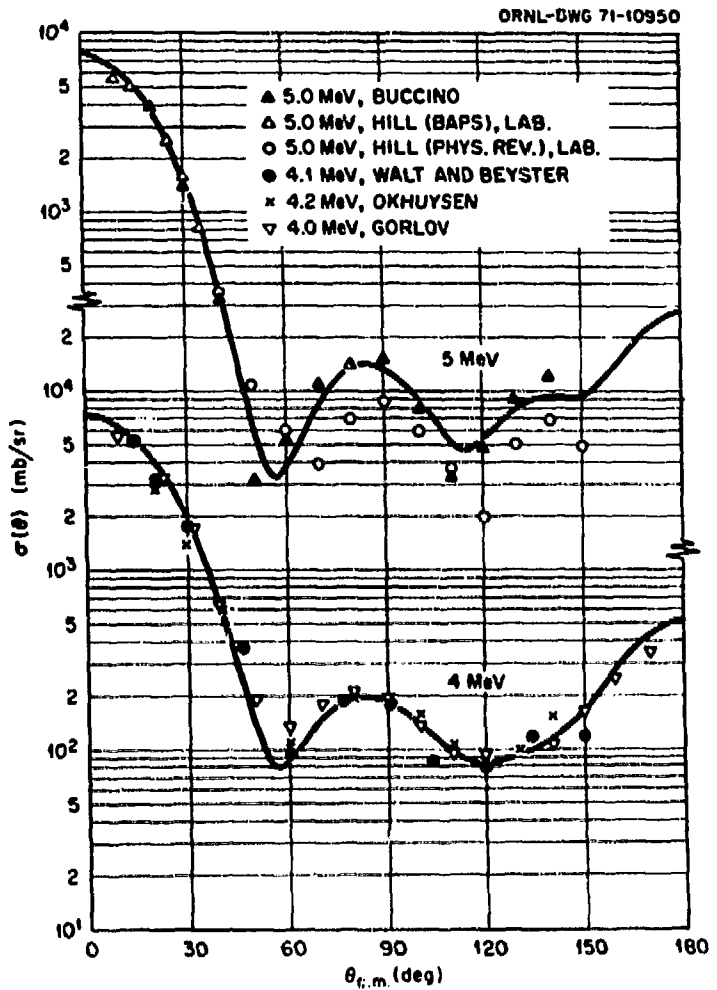
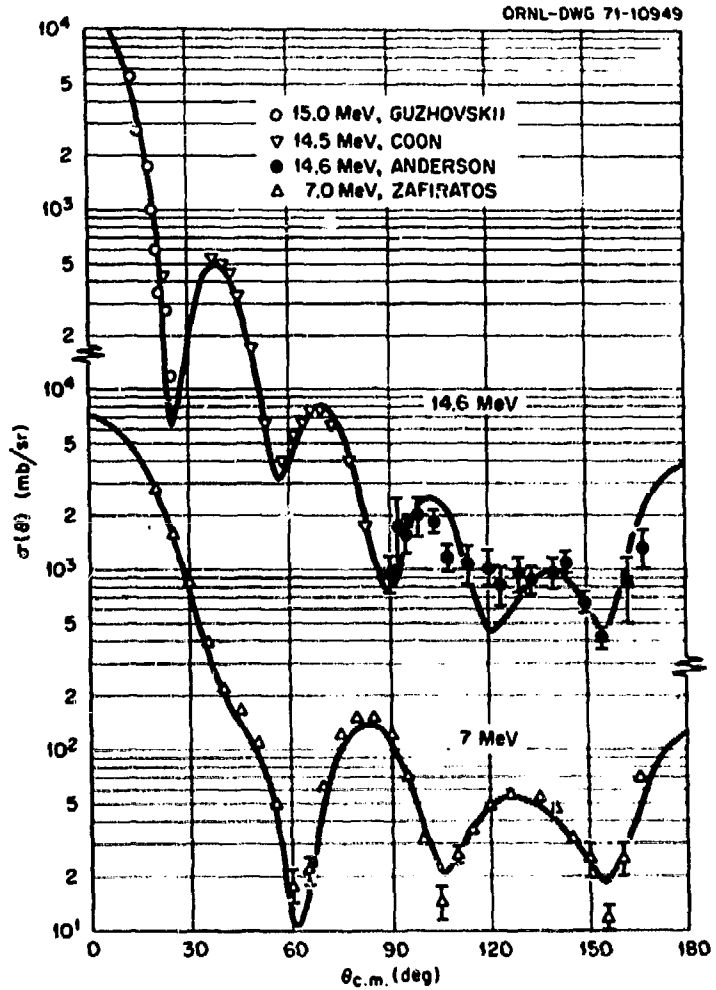


FIGURE 13

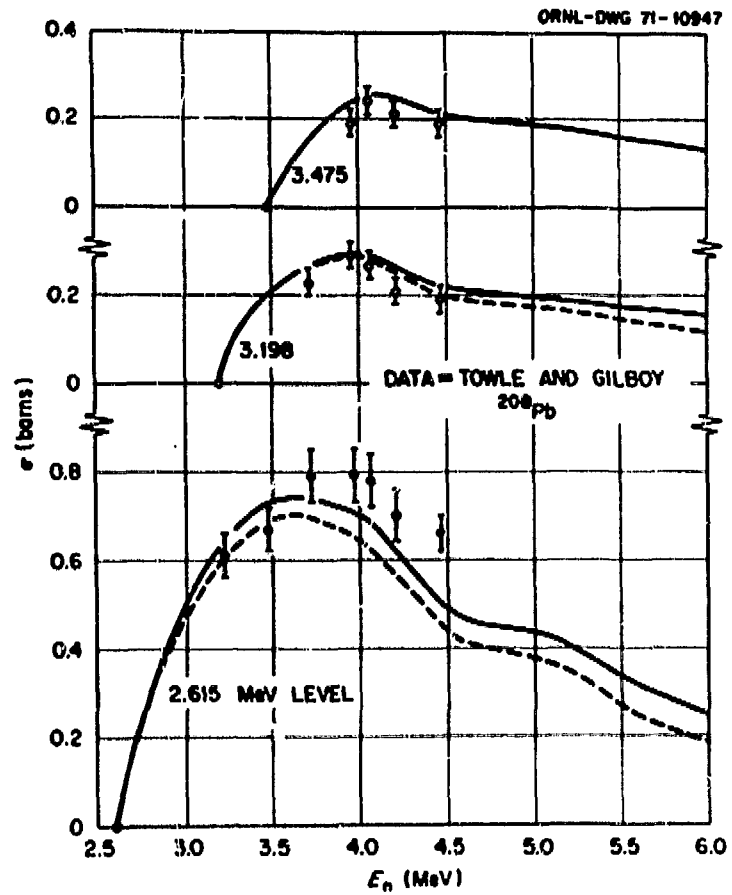
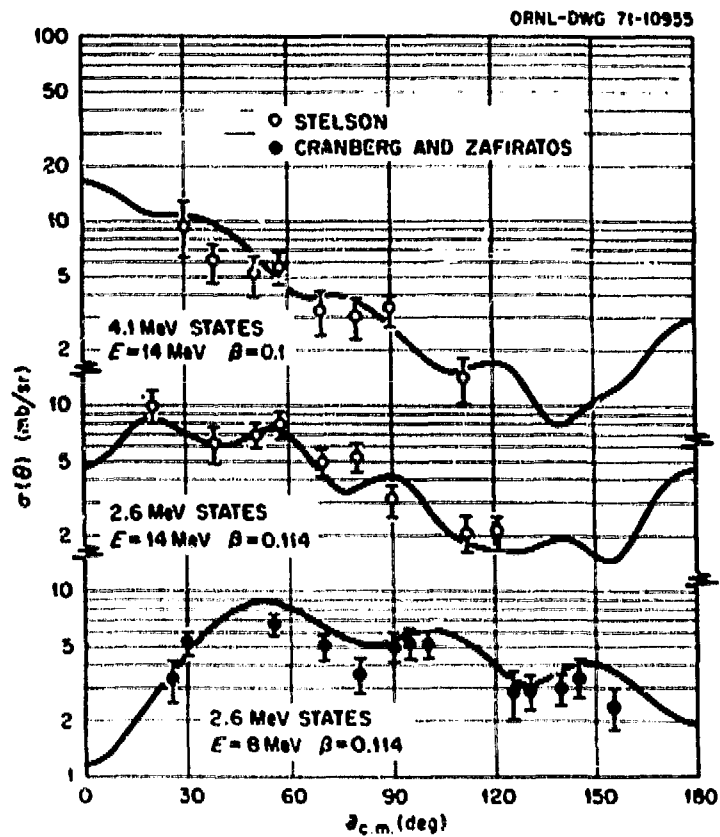


FIGURE 14

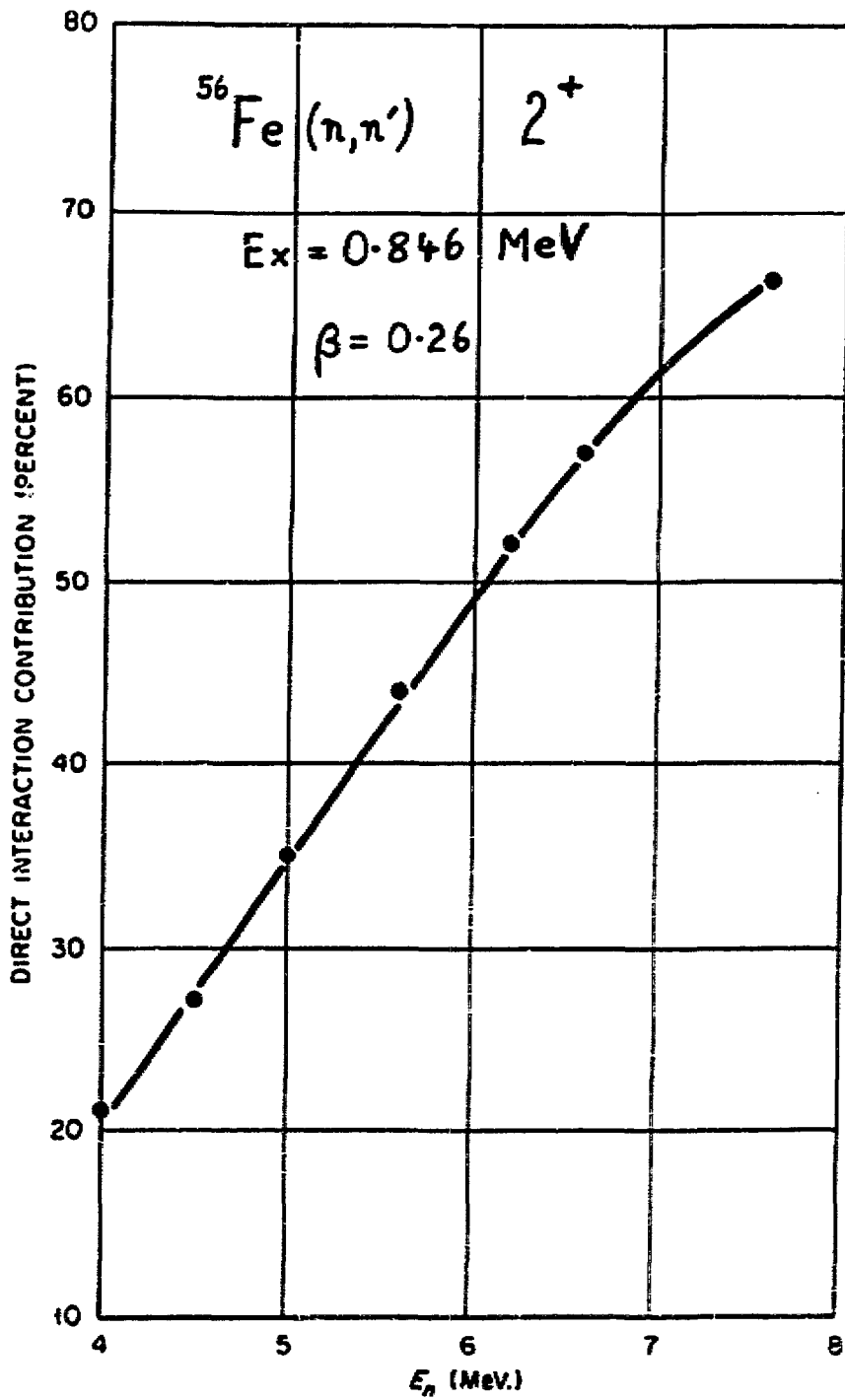


FIGURE 15

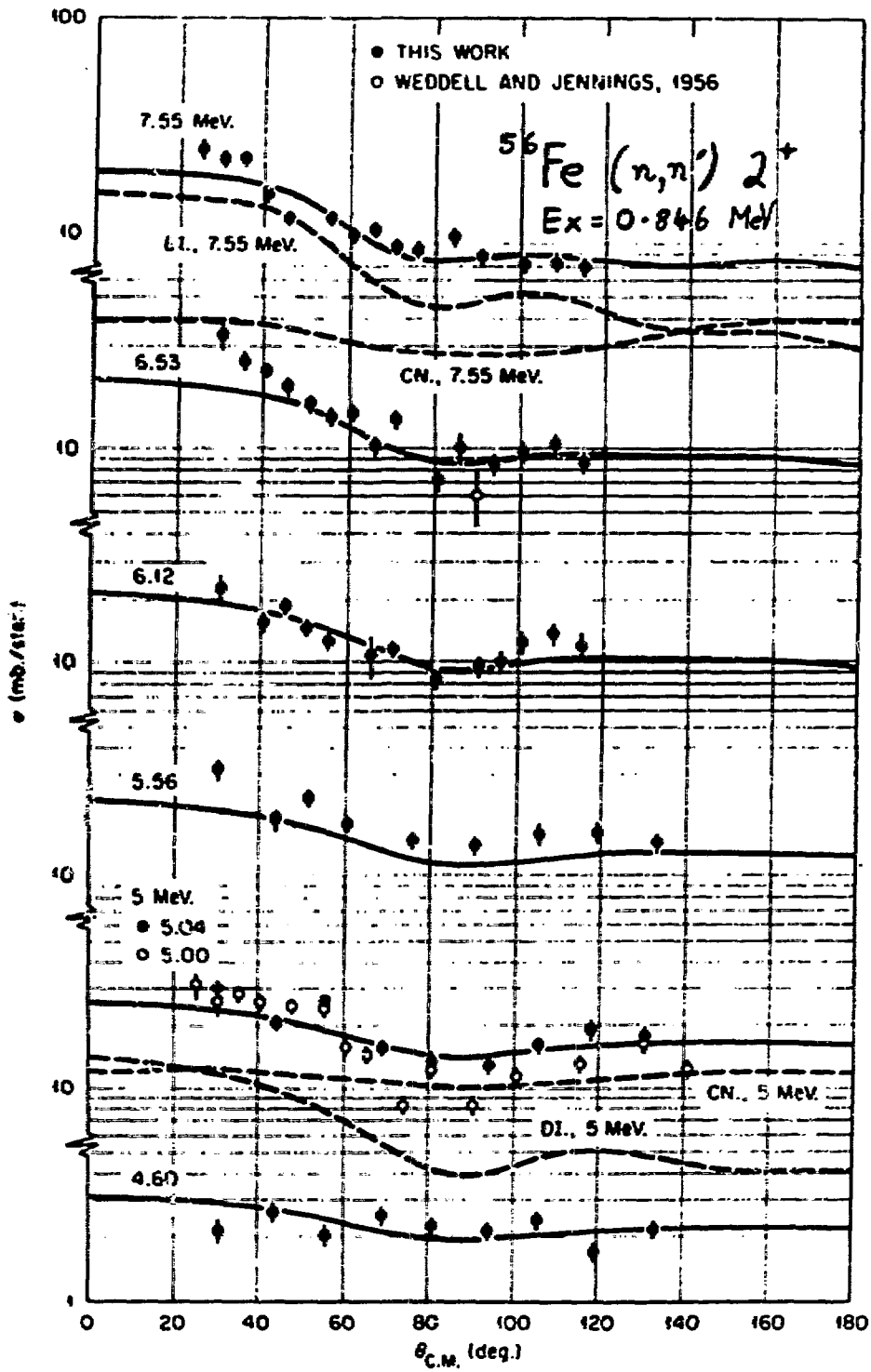


FIGURE 16

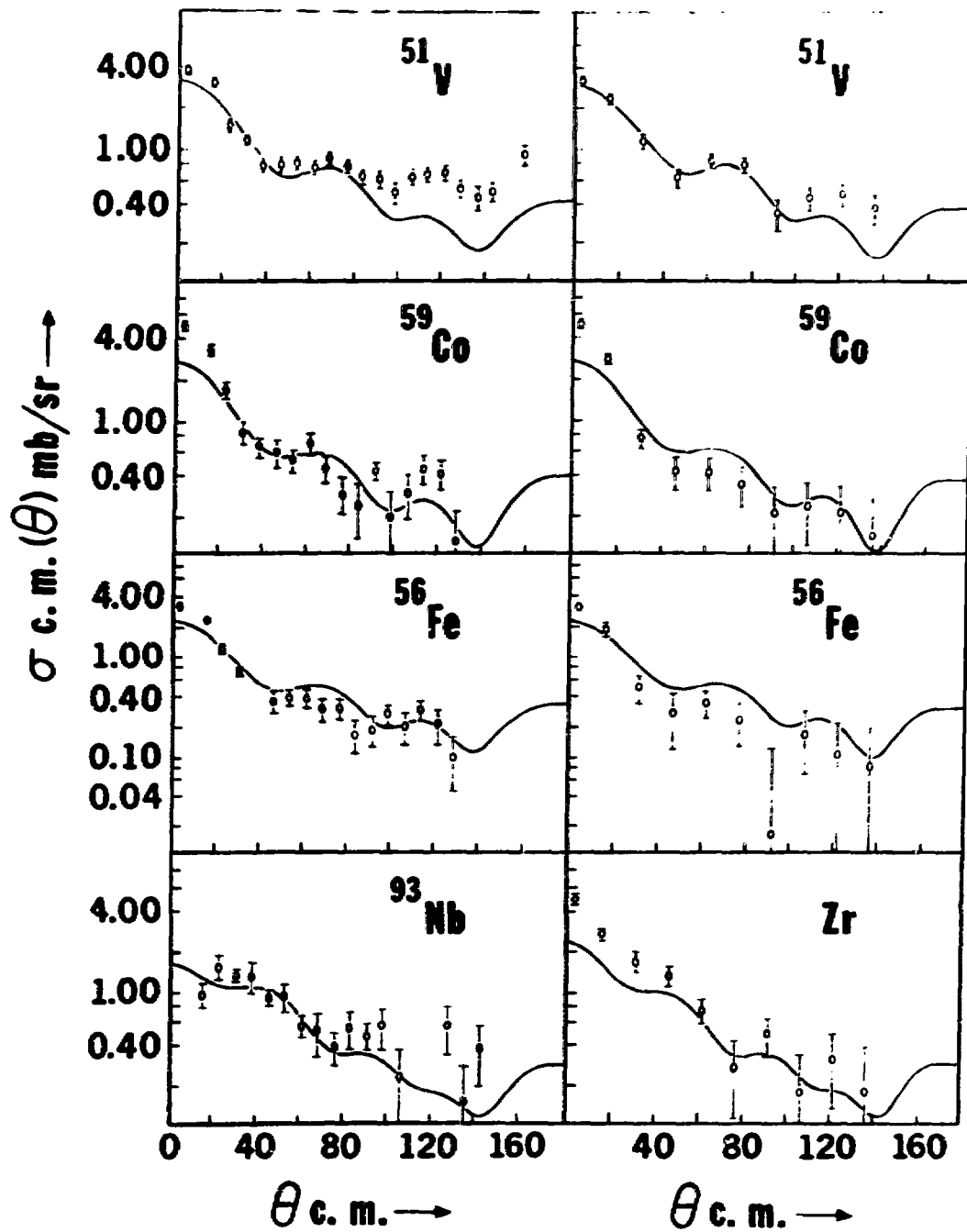


FIGURE 17

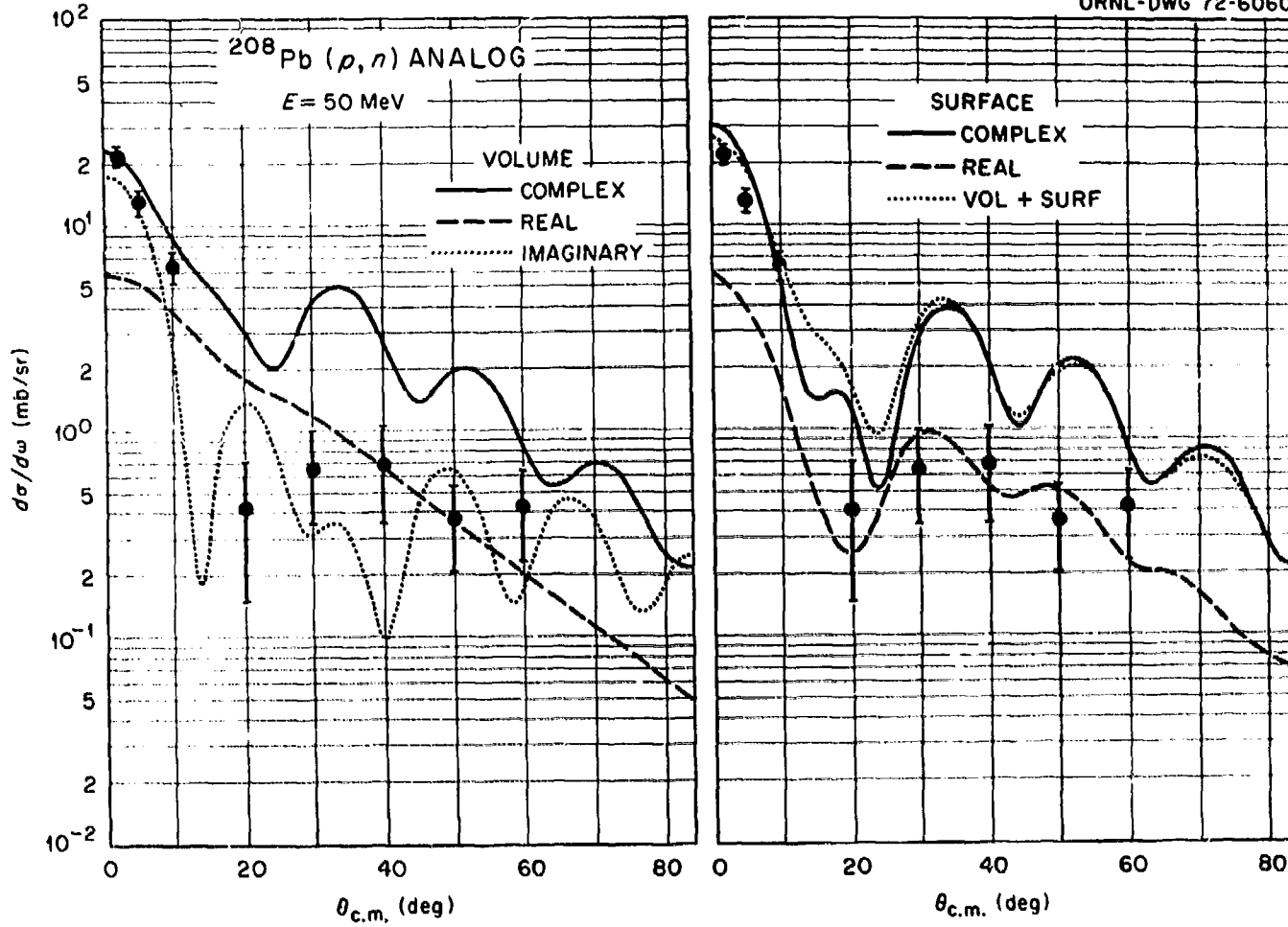


FIGURE 18

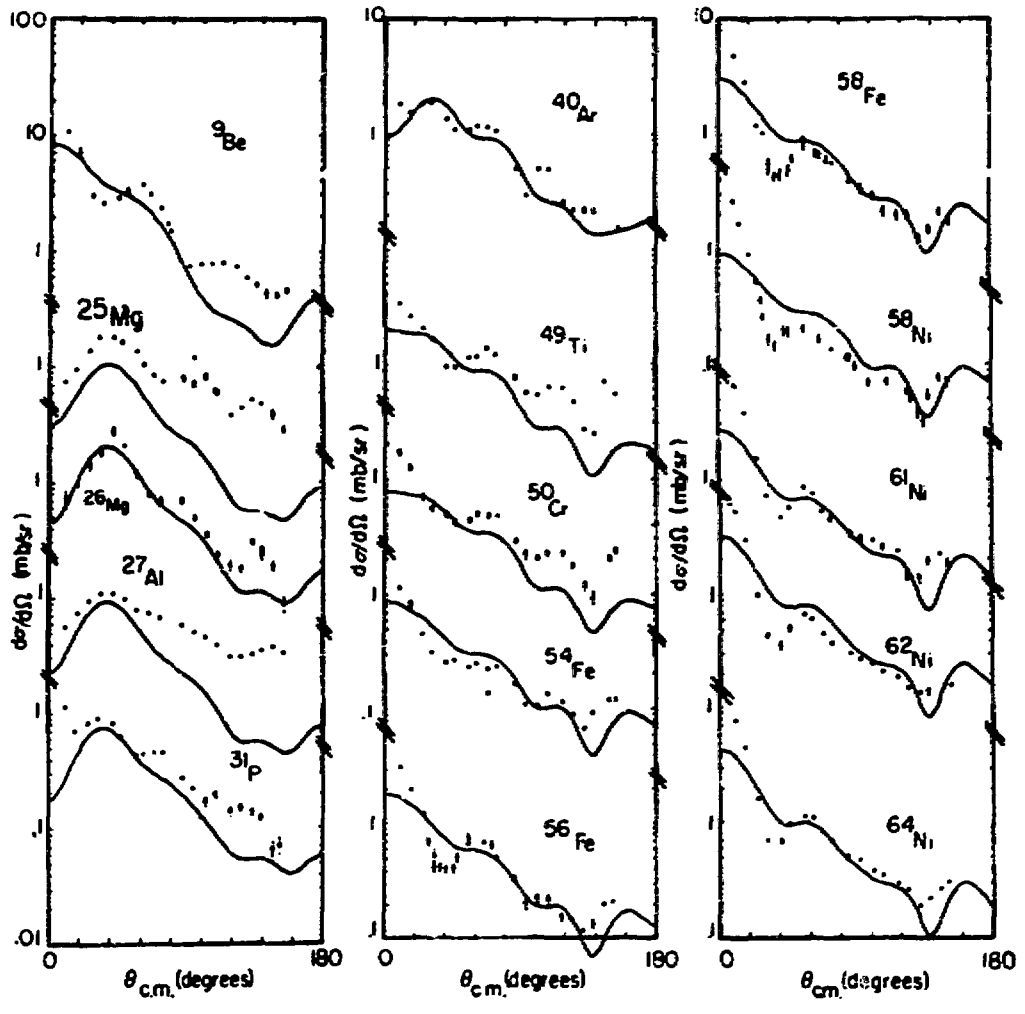


FIGURE 19

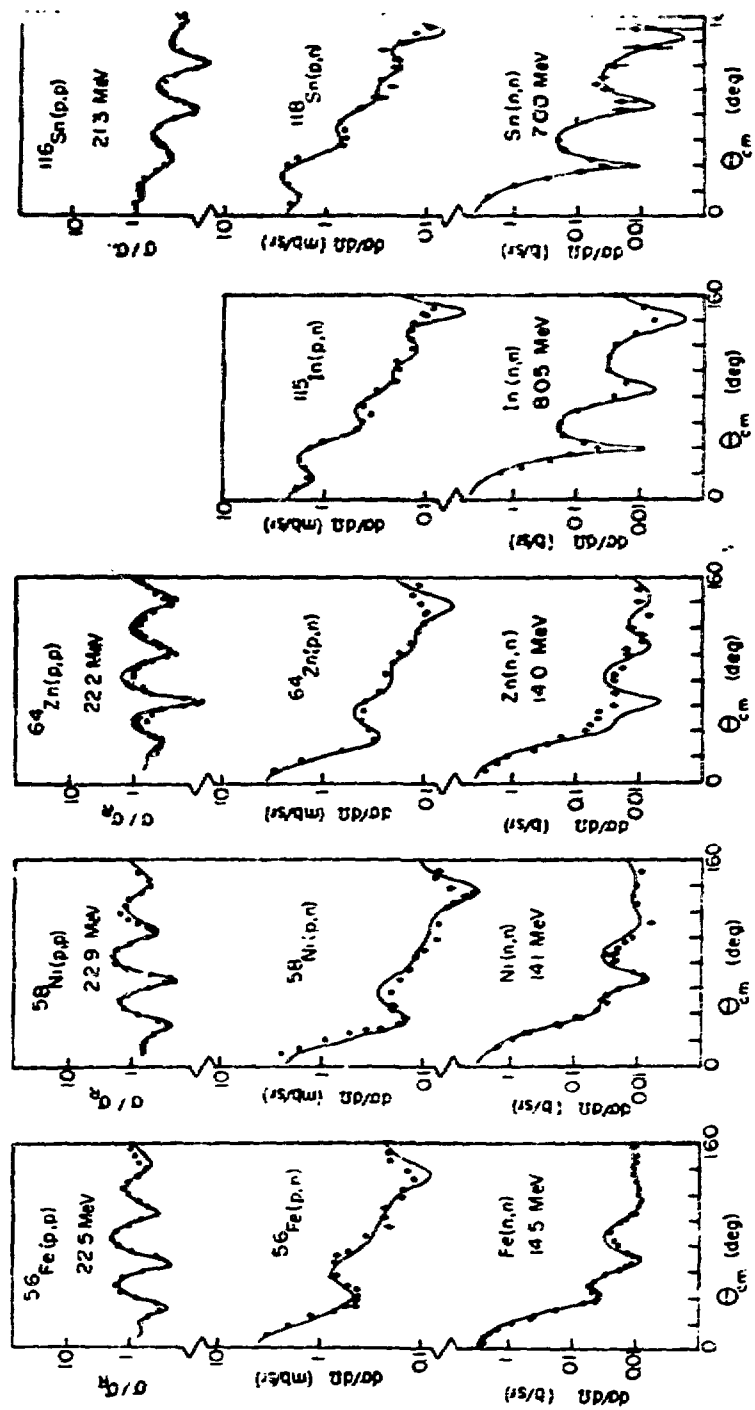


FIGURE 20

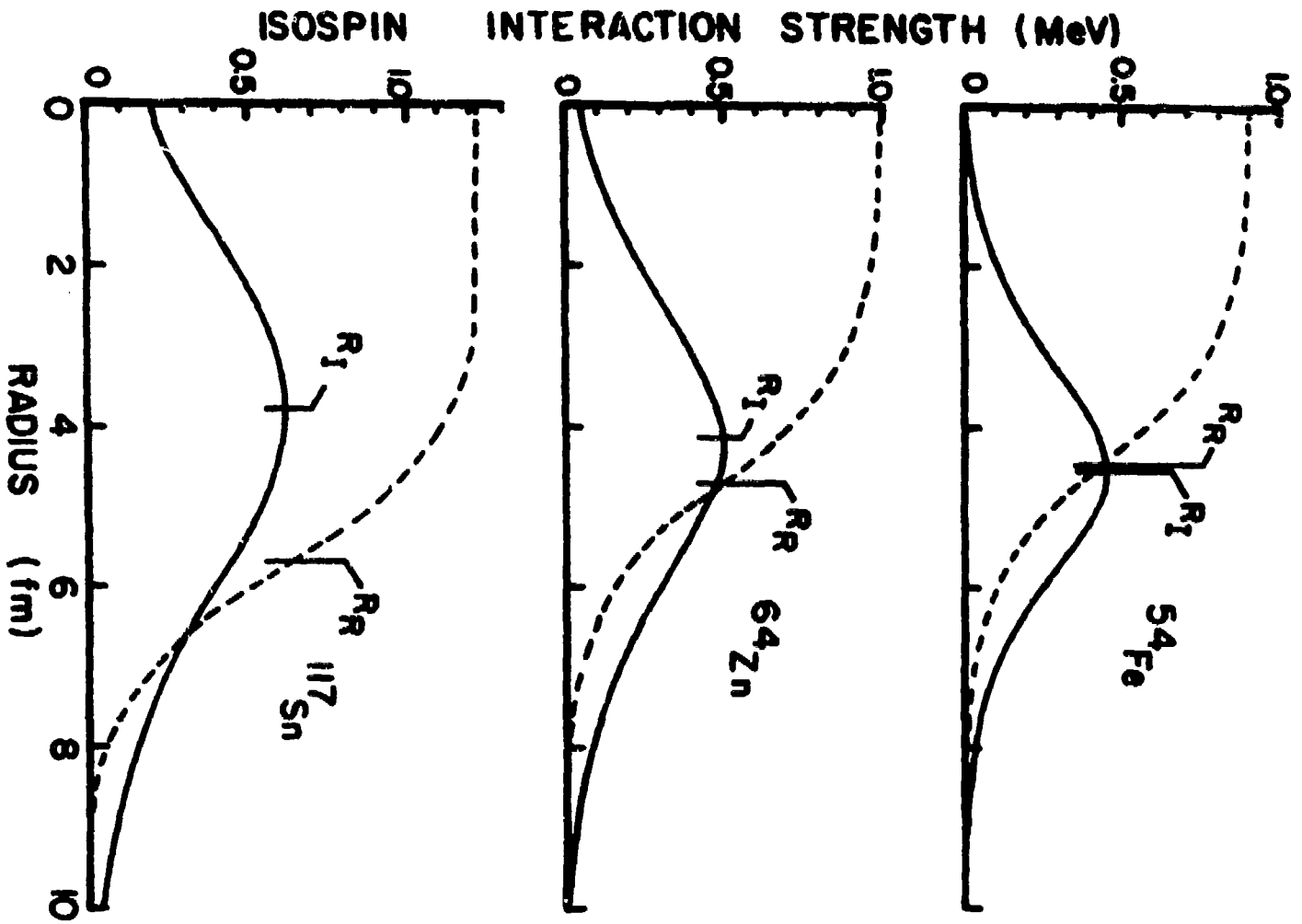


FIGURE 21

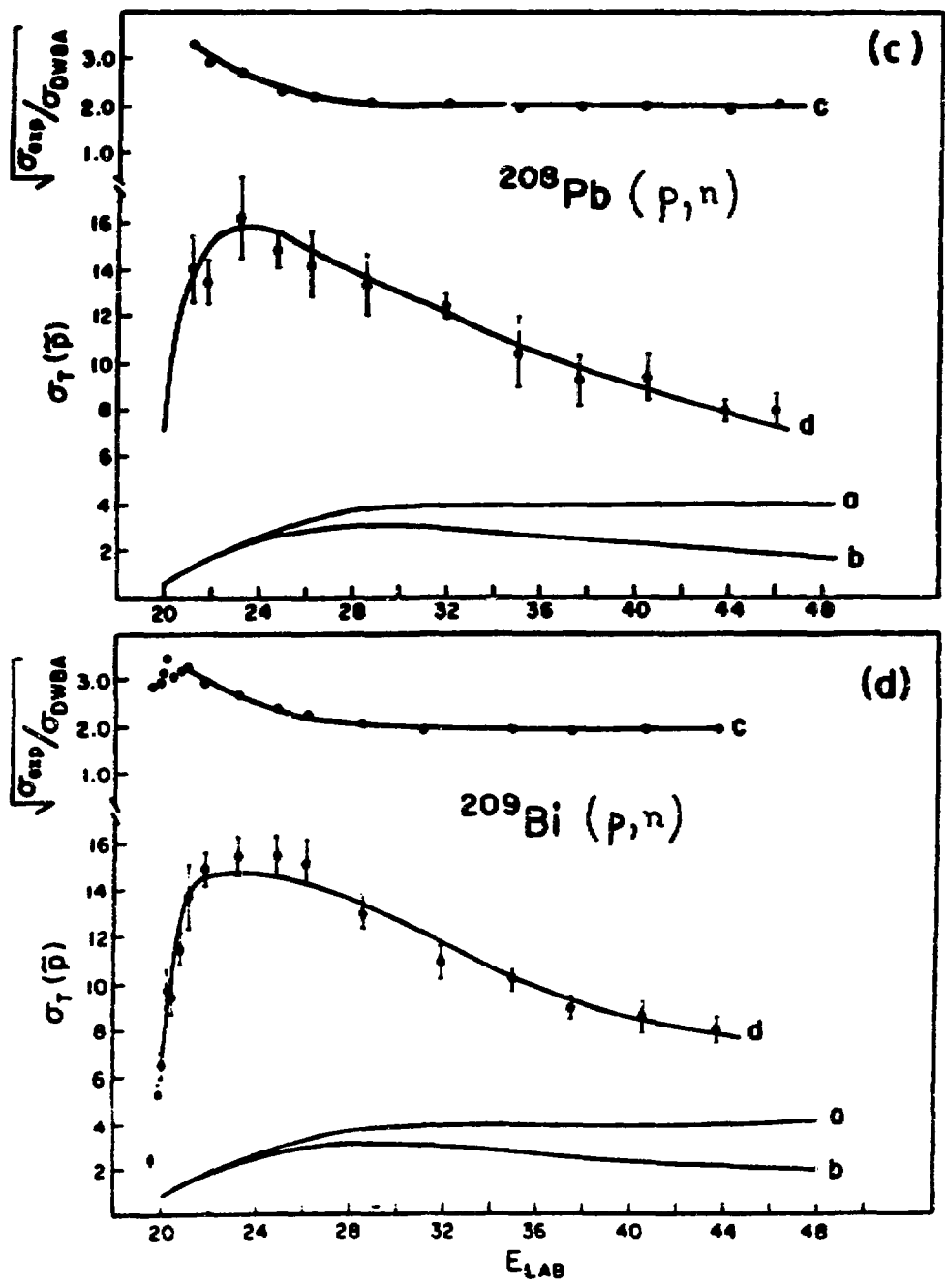


FIGURE 22

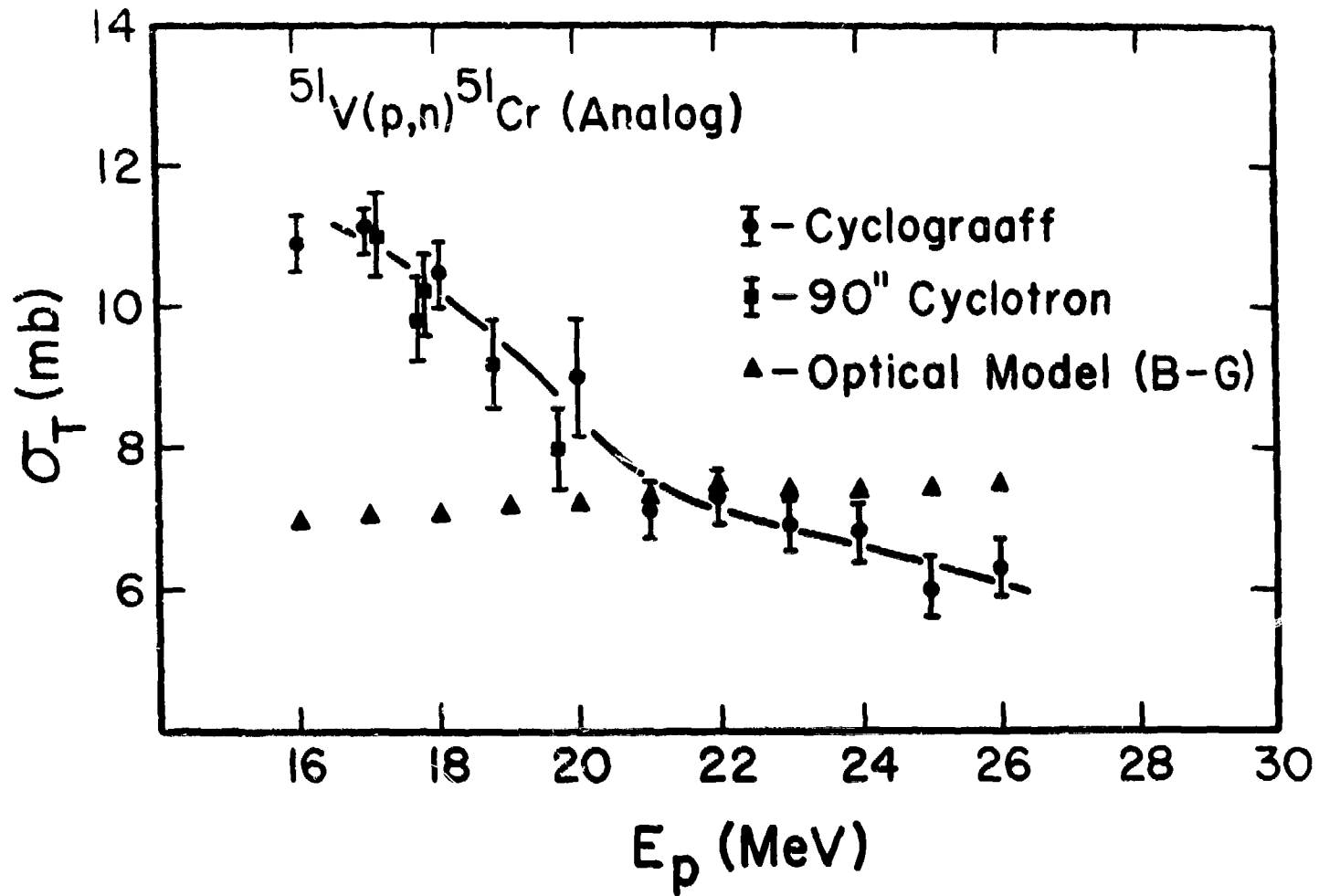


FIGURE 23

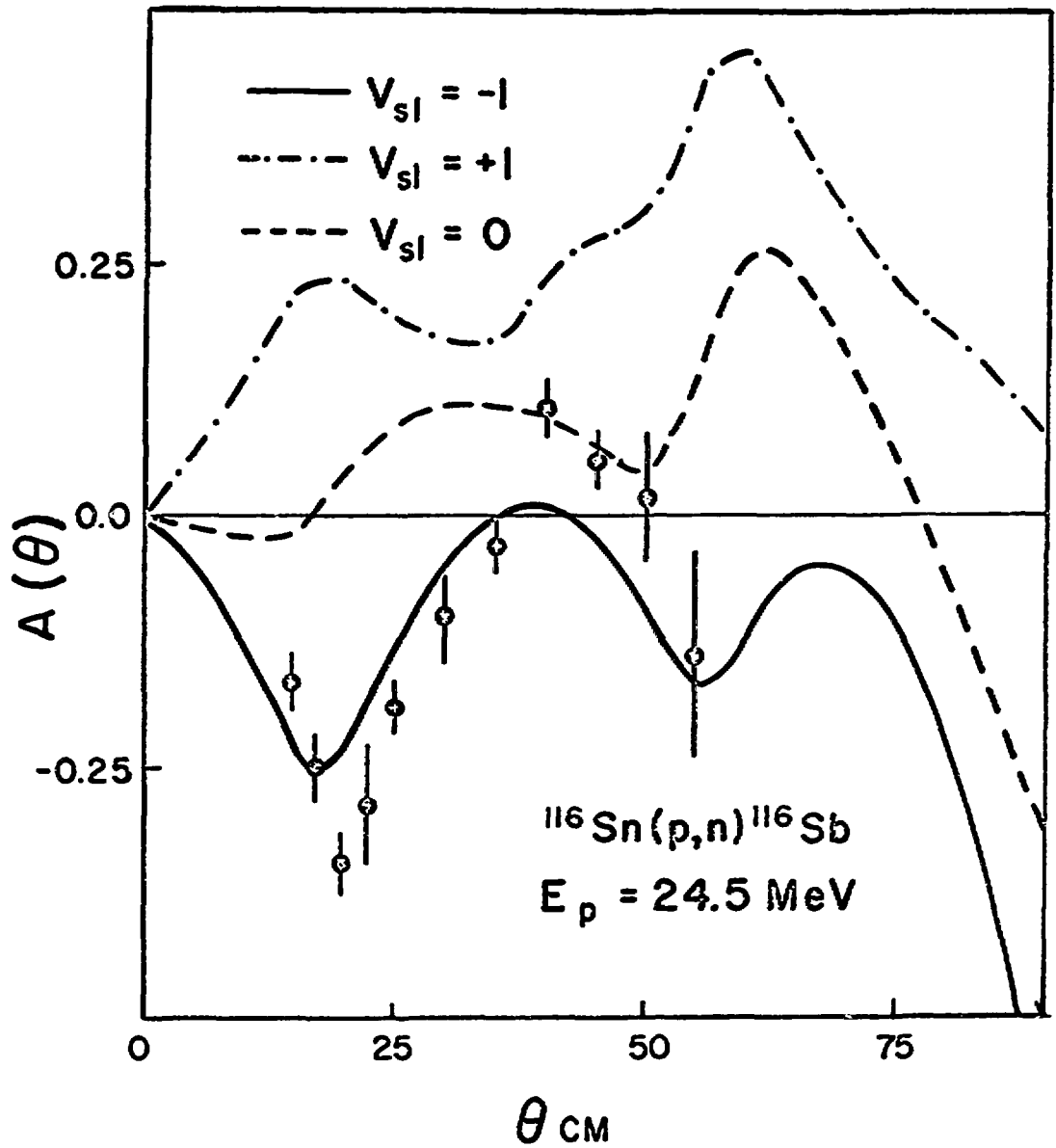


FIGURE 24

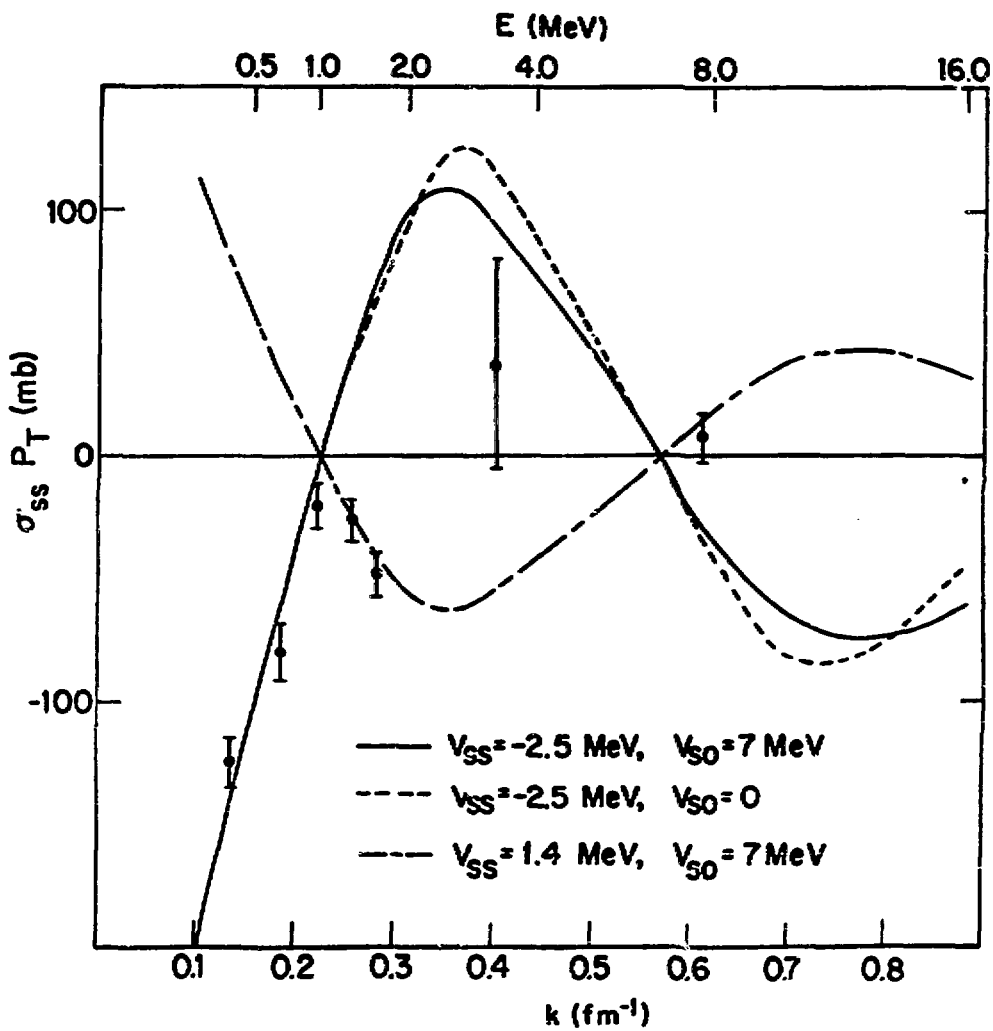


FIGURE 25

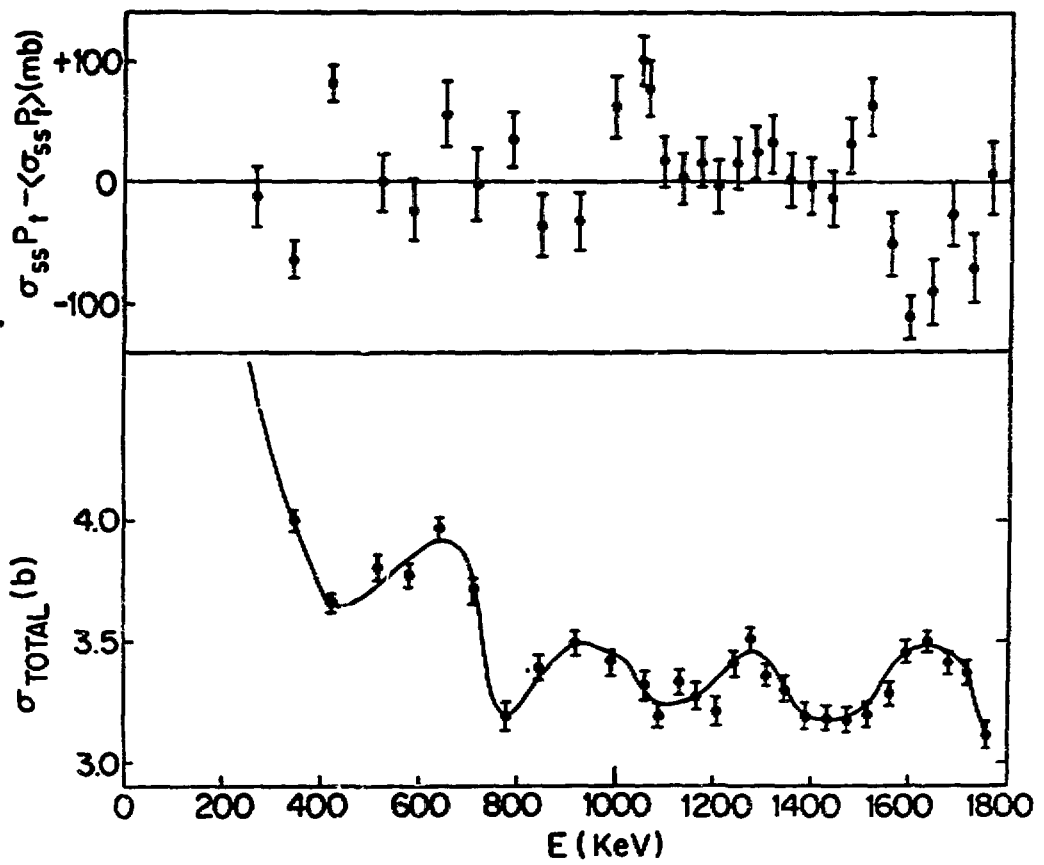


FIGURE 26

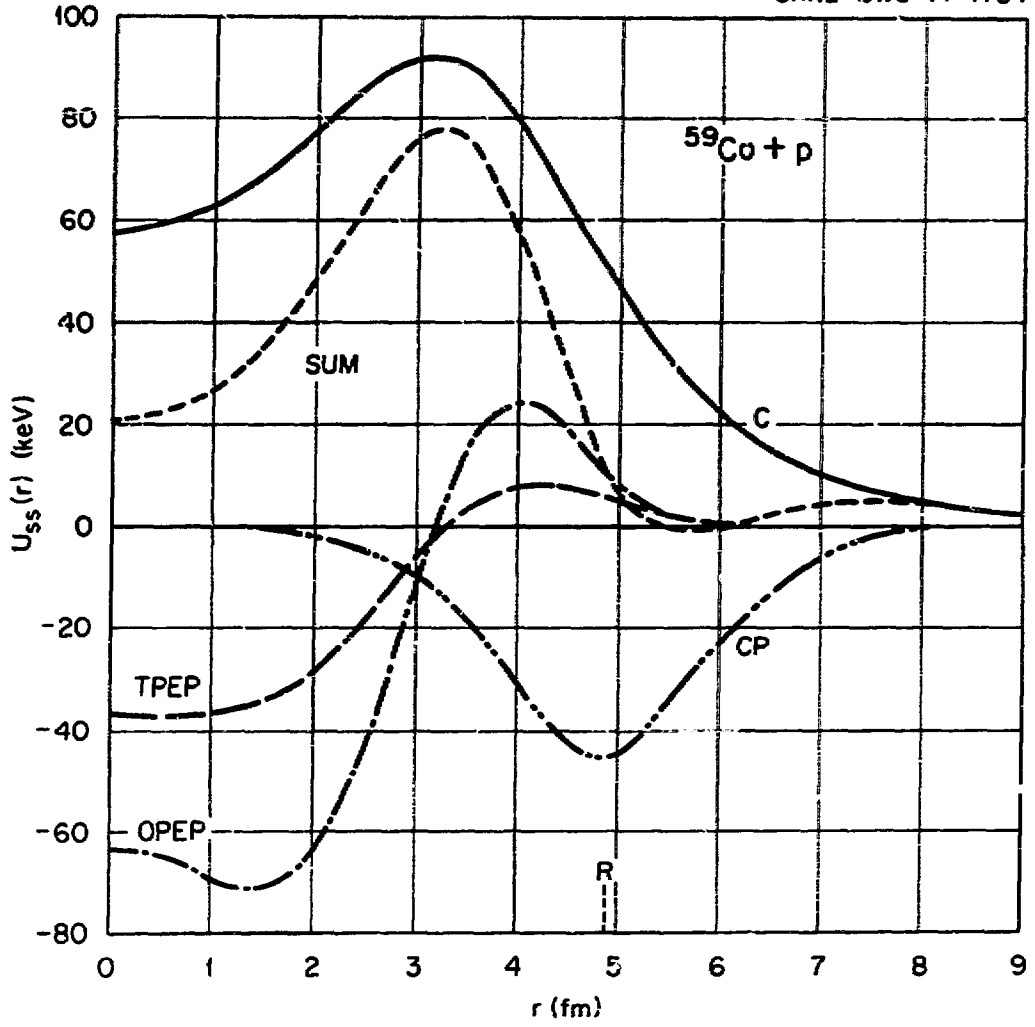
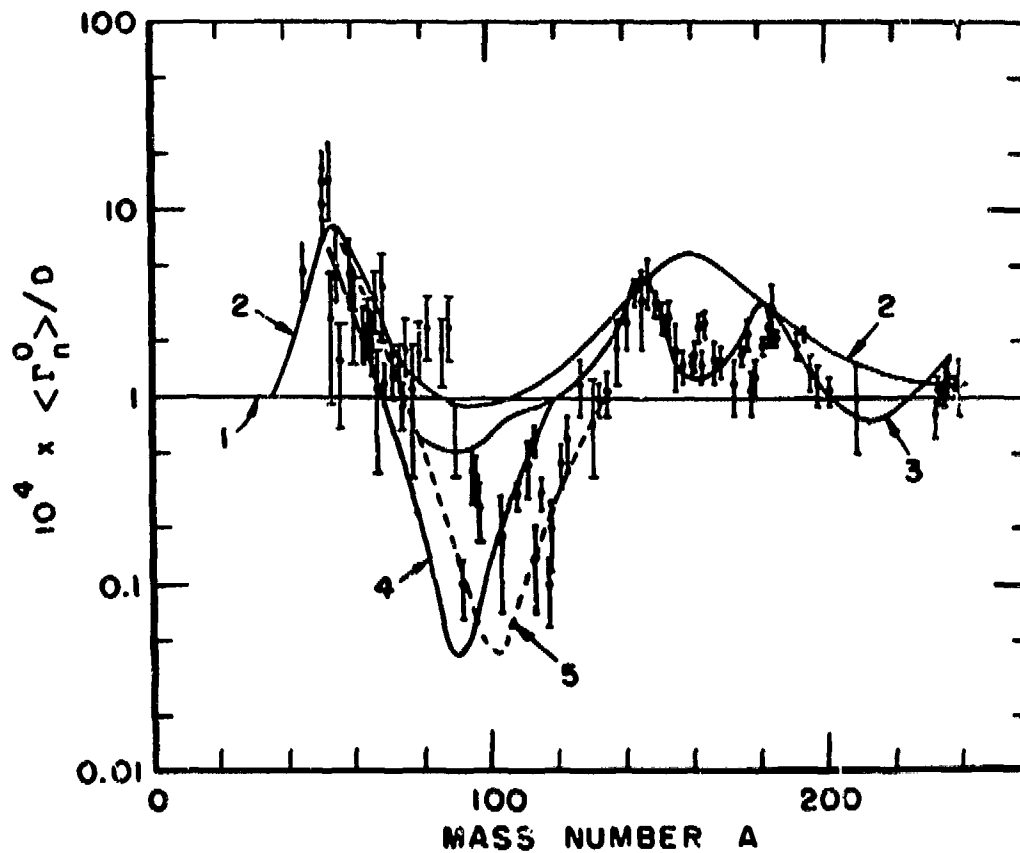


FIGURE 27

END -- DATE FILMED



Sensitivity of S-wave neutron strength function to details of the optical potential. Curve 1: black nucleus; 2: volume absorption; 3: spherical potential; 4: thin surface absorptive shell; 5: absorptive shell of greater radius.

FIGURE 28

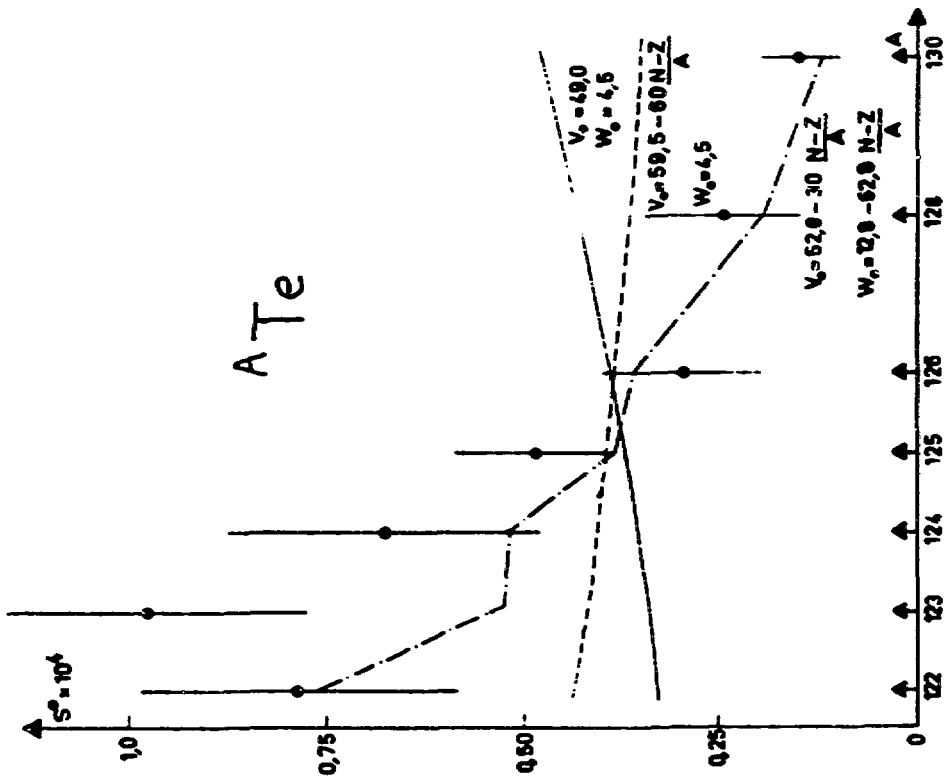


FIGURE 29

11 / 9 / 72